



Organic carbon pathways across the fluvial-marine transition zone of the Mackenzie River Delta - Beaufort Sea region and implications on ocean color remote sensing

Annabeth McCall^{1,2}, Martin Hieronymi³, P. Paul Overduin¹, Lisa Bröder⁴, Julie Lattaud^{5,6}, Rüdiger Röttgers³, Irina Overeem⁷, Anne Morgenstern¹, Guido Grosse^{1,2}, Bennet Juhls¹

¹Alfred Wegener Institute Helmholtz Centre for Polar and Marine Research, Potsdam, Germany

²Institute of Geosciences, University of Potsdam, Potsdam, Germany

³Institute of Carbon Cycles, Helmholtz-Zentrum Hereon, Geesthacht, Germany

⁴Department of Earth and Planetary Sciences, Geological Institute, ETH Zürich, Zürich, Switzerland

10 ⁵Department of Environmental Science, Stockholm University, Stockholm, Sweden

⁶Bolin Center for Climate Research, Stockholm, Sweden

⁷Institute of Arctic and Alpine Research, University of Colorado, Boulder, Boulder, USA

Correspondence to: Annabeth McCall (annabeth.mccall@awi.de)

15 **Abstract.** Arctic warming and hydrological intensification are accelerating permafrost thaw and increasing the export of terrestrial organic carbon (OC) and sediments from land via rivers and shallow coastal waters into marine waters, yet the fate of these materials in deltaic and coastal transition zones remains poorly understood. Here, we synthesize multiyear in situ biogeochemical, optical, and radiometric observations (2009–2024) across the Mackenzie River Delta–southern Beaufort Sea land–ocean continuum. By using a compartmental approach (river, delta, coastal, marine) we quantify spatial and seasonal
20 variability in dissolved organic carbon (DOC), particulate organic carbon (POC), and suspended particulate matter (SPM) and refine bio-optical relationships that support satellite retrievals in optically complex Arctic waters. Our results show that DOC concentrations declined from river to marine waters (mean 4.8 to 1.9 mg L⁻¹), while POC and SPM showed more variability with marked reductions across the transition, consistent with retention and transformation processes in deltaic and nearshore zones. Across all compartments, DOC exhibited a strong non-linear relationship with CDOM absorption at 443 nm
25 ($a_{\text{CDOM}(443)}$; $r^2=0.81$), whereas POC related linearly to particulate absorption at 443 nm ($a_{\text{P}(443)}$; $r^2=0.73$), with substantial compartment dependent differences in slope and fit strength that indicate shifting OC composition and optical regimes along the salinity gradient. Optical Water Type (OWT) classification derived from remote sensing reflectance (R_{rs}) resolved transitions from turbid, particle-dominated waters to clearer coastal and marine regimes, providing a framework for guiding algorithm selection and improving retrieval performance. These results provide the first concurrent, Arctic fluvial-marine
30 assessment of DOC, POC, SPM, and optical properties and demonstrate how land–sea connectivity governs both organic carbon processing and optical structure in Arctic coastal waters.



1. Introduction

Increasingly warmer temperatures in the Arctic have led to accelerated permafrost thaw and mobilization of previously sequestered terrestrial soil organic carbon (Schuur et al., 2015). Coupled with increasing precipitation (Rapačić et al., 2015) and consequently increasing riverine discharge (Peterson et al., 2002; Holmes et al., 2011) the transport of terrestrial organic matter into the aquatic system and into coastal waters is intensifying across major Arctic watersheds (Holmes et al., 2011; Clark et al., 2022). As fresh riverine water mixes with saline ocean water in deltaic and coastal transition zones, strong gradients in salinity, turbidity, and light availability drive biogeochemical transformations including photochemical and microbial degradation (Holmes et al., 2011, Juhls et al., 2019), remineralization and flocculation (Eisma, 1986) occur. These processes regulate the fate of terrestrial matter along the Arctic land-ocean continuum (Holmes et al., 2011; Clark et al., 2022) and ultimately influence regional carbon cycling and climate feedbacks. Among these systems, the Mackenzie River Delta–Beaufort Sea region represents one of the largest and most dynamic fluvial–marine transition zones in the Arctic, characterized by strong sediment loads, extensive permafrost influence, and pronounced optical variability, making it an ideal natural laboratory to investigate organic carbon and sediment pathways from land to ocean.

Deltaic and shallow coastal waters function as critical biogeochemical filters that modulate the quantity and quality of organic matter and sediments exported to the Arctic Ocean (AO). Accelerated warming (Rantanen et al., 2022), permafrost thaw (Biskaborn et al., 2019) and coastal erosion (Irrgang et al., 2022; Nielsen et al., 2022) in the Arctic enhance sediment and carbon delivery to these transition zones, potentially increasing biogeochemical transformation and altering the balance between carbon storage and atmospheric CO₂ exchange. Recent studies suggest that terrestrial inputs may reduce the AO's net CO₂ sink strength by 7-14 % (Nielsen et al., 2022) and can turn coastal shelf regions into local CO₂ sources (Bertin et al., 2023; Oziel et al., 2025). Despite their importance, shallow coastal and deltaic waters remain sparsely sampled and observed, limiting our ability to resolve how land–sea connectivity controls carbon pathways and fluxes in a rapidly changing Arctic system (Holmes et al., 2011; Zhang et al., 2021).

The magnitude and fate of exported carbon depend strongly on its composition and transport history. OC carbon exported from rivers to the ocean varies widely in both origin and composition, reflecting watershed hydrology and geomorphology, and permafrost influence (Lynch et al., 2019; Clark et al., 2022). Although dissolved and particulate fractions of OC originate from similar terrestrial sources, for instance vascular plant degradation, soil leaching, and terrigenous erosion, they respond differently to transport and mixing processes along the fluvial–marine continuum (Clark et al., 2022). Studies across Arctic river systems have shown that high river discharge conditions preserved the quality of dissolved organic matter (DOM), while low flow conditions in summer allowed for significant microbial and photochemical degradation (Novak et al., 2022). In parallel, particulate organic carbon (POC) undergoes substantial modification through sedimentation, resuspension, and sorting processes during downstream transport and across deltaic transition zones (Ogneva et al., 2023; McClelland et al., 2016). These combined processes influence both the concentration and optical properties of organic matter delivered to Arctic shelf seas. Similarly, Juhls et al. (2019) showed modifications of terrigenous DOM across the Lena-Laptev Sea transition zone with



65 subsequent work revealing pronounced seasonal and salinity-dependent variability in dissolved organic carbon (DOC) concentrations and optical properties on the Beaufort Sea shelf (Juhls et al., 2022).

Across fluvial-marine gradients, changes in organic matter and sediment composition are closely linked to shifts in optical properties of the water. The absorption of colored dissolved organic matter $a_{CDOM}(\lambda)$ and particulates $a_P(\lambda)$ provide measurable proxies for DOC and POC concentrations, and form the basis for Ocean Color Remote Sensing applications in Arctic waters
70 (Gonçalves-Araujo et al., 2015; Juhls et al., 2019; Matsuoka et al., 2012; Matsuoka et al., 2017; Pugach et al., 2018; Juhls et al., 2022). These bio-optical relationships enable synoptic monitoring of surface water properties at high temporal resolution and have supported regional retrieval algorithms for DOC, POC, and suspended particulate matter (SPM) across Arctic river-influenced shelves (Doxaran et al., 2012; Matsuoka et al., 2017; Matsuoka et al., 2022; Juhls et al., 2022; Tarasenko et al., 2023). However, the robustness and accuracy of satellite retrievals depends on transferable relationships between
75 biogeochemical and bio-optical properties which still remains poorly constrained across the full river-delta-coastal-offshore continuum (Doxaran et al., 2012).

Satellite-based observations suggest substantial long-term changes in the Mackenzie Beaufort Land-Ocean transport, including a ~50 % increase of terrestrial SPM flux (Doxaran et al., 2015), and a 57 % increase in POC and 8 % increase in DOC concentrations (Matsuoka et al., 2022). Complementary in situ measurements indicate a 39 % increase in DOC flux over the
80 past four decades, likely linked to permafrost thaw (Tank et al., 2016). Reduced sea ice cover coupled with strong CDOM absorption can lead to water darkening and altered surface heating (van Oostende et al., 2023). In contrast to earlier studies, a more recent study by Tarasenko et al. (2023) reported decreasing SPM concentrations. This divergence highlights the optical complexity of fluvial-marine transition zones where waters shift from highly scattering sediment-rich plumes to more absorbing CDOM-rich and then ultimately clearer oceanic regimes. Such variability pushes satellite algorithms beyond their
85 optimal ranges and underscores the need for more consistent in situ validation and improved reliability of remote sensing-based assessments in these dynamic Arctic coastal environments. Region-specific challenges further complicate remote-sensing applications. During winter, the absence of sunlight precludes optical observations, while during the short open-water season persistent cloud cover and low solar elevation angles increase atmospheric path lengths and introduce uncertainties in remote-sensing reflectance (R_{rs}), the fundamental input for constituent retrievals. In addition, the lack of spatially resolved,
90 parallel measurements of biogeochemical, bio-optical, and radiometric properties across salinity gradients limits efforts to validate and operationalize satellite-based estimates of DOC, POC, and suspended particulate matter across the river-delta-coastal continuum. As rivers deliver seasonally varying mixtures of sediments, dissolved and particulate constituents to coastal waters (Holmes et al., 2011), optical properties evolve across ocean, coastal, and inland waters (Xi et al., 2013) and directly influence the spectral characteristics and consequently the remote-sensing reflectance (R_{rs}) (Bi & Hieronymi, 2024). Optical
95 water types (OWTs) classification provides a framework to interpret this variability by linking spectral reflectance patterns to dominant optical regimes, narrowing the down of corresponding concentration range of optically active water constituents. By integrating in situ observations with bio-optical characterization, we can bridge the existing gap between point-scale biogeochemical observations and synoptic-scale satellite monitoring.



100 Despite these advances, Arctic shallow coastal and deltaic waters remain under-sampled. In particular, the lack of spatially resolved parallel sampled biogeochemical, bio-geo-optical and radiometric data across the salinity gradients limits efforts to validate and operationalize satellite-based matter flux estimates. These areas are central to understanding how changes will impact the pan-Arctic carbon budget and source-to-sink dynamics, yet are often excluded from monitoring programs due to accessibility and cost constraints. Without improved observations and process understanding in these transition zones, monitoring and modelling of carbon fluxes at relevant spatial and temporal scales remains limited.

105 Within this broader Arctic context, the Mackenzie-Beaufort Sea system provides an ideal setting to examine organic carbon and sediment pathways across fluvial-marine compartments. Here, we i) quantify seasonal and spatial variability of DOC, POC, and SPM across four aquatic compartments: river, delta, coastal, and marine waters, ii) establish refined empirical relationships between optical properties and OC, and iii) test and apply OWT classification for improving satellite retrieval accuracy in optically complex Arctic waters. By synthesizing biogeochemical, optical and radiometric datasets collected
110 between 2009 and 2024 across river, delta, coastal, and marine compartments, this study links organic carbon and sediment transport to optical regimes and provides new constraints for regional satellite retrieval approaches. This work presents the first synthesis to concurrently quantify DOC, POC, SPM, and optical properties across all major compartments of the Mackenzie River Delta–Beaufort Sea fluvial–marine continuum.

2. Materials and methods

115 2.1 Study area and expeditions

This study focuses on the land–ocean interface of the Mackenzie River Delta–southern Beaufort Sea, a fluvial-dominated delta draining the largest watershed in Canada (1.8 million km²). The basin spans the full permafrost gradient, from continuous to discontinuous and sporadic permafrost zones with approximately 13 % underlain by continuous permafrost and 42 % by continuous and discontinuous permafrost combined, of which approximately 80 % is underlain by permafrost (Woo and
120 Thorne, 2003; Holmes et al., 2011; Elshamy et al., 2025) (Fig. 1a). This broad permafrost transition exerts strong controls on hydrology, sediment delivery, and organic carbon composition entering the delta-shelf system. The Mackenzie River is characterized by strong seasonality in discharge and its water biogeochemistry (Fig. 2). Discharge observations used for this study were collected from the Mackenzie-Red River gauge station at Tsiigehtchic, part of the Arctic Great Rivers Observatory (ArcticGRO) long-term monitoring effort (arcticgreatrivers.org). The hydrography of the Mackenzie
125 River can be described in three periods: spring ice break-up, summer to autumn months, and winter. For the purpose of this study, we will focus on the ice-free summer and autumn months (June through October).

The in-situ data presented in this study are synthesized from several datasets from both ship and land-based expeditions to the Mackenzie River Delta and Beaufort Sea that took place from 2009 to 2024: MALINA 2009 (Massicotte et al., 2021) , Nunataryuk 2019 (Lizotte et al., 2023), PeCaBeau 2021 (Bröder et al., 2022), and FLOCHAR 2024 (this study), in addition to
130 two stationary long-term sampling efforts, ArcticGRO and Mackenzie Monitoring (mackenzie-monitoring.awi.de). Table 1



shows a summary of sampling periods, sample/data types and the measured parameters of individual campaign datasets. Sampling locations from these datasets include large parts of the Beaufort Shelf, shallow coastal waters around the Mackenzie Delta including Kugmallit Bay and Shallow Bay, and channels and distributaries of the Mackenzie River (Fig. 1b). These data were collected at various levels of river discharge (Fig. 2) where 2024 exhibited drought conditions (purple hydrograph) and 2021 exhibited high flow year (red hydrograph). The variations exhibited by the Mackenzie River over the sampling periods allow us to investigate the influence of discharge on transport and transformation of carbon from land to sea.

Table 1. Sampling period, sample type and measured parameters of datasets used in this study.

Campaign	Dataset Description	Location	Year & Period	Type	No. of observations	Parameters
MALINA	Massicotte et al., 2021	Southern Beaufort Sea	2009; Summer	Water samples, optical data, radiometric data	91	DOC, POC, SPM, a_{CDOM}^a , a_P^b , R_{rs} , conductivity
Nunataryuk	Lizotte et al., 2023	Mackenzie Delta and Shallow Bay	2019; Summer to Autumn	Water samples, optical data, radiometric data	79	DOC, POC, SPM, a_{CDOM}^a , a_P^b , R_{rs} , conductivity
PeCaBeau	Bröder et al., 2022	Southern Beaufort Sea	2021; Summer	Water samples, optical data, radiometric data	20	DOC, POC, SPM, a_{CDOM}^a , a_P^b , R_{rs} , conductivity
FLOCHAR	This study	Mackenzie Delta and Kugmallit Bay	2024; Summer	Water samples, optical data, radiometric data	70	DOC, POC, SPM, a_{CDOM}^a , a_P^b , R_{rs} , conductivity
ArcticGRO	Arctic Great Rivers Observatory, https://www.arcticgreatrivers.org/data	Mackenzie River at Tsiighetchic	1974-present; year round	Water samples	118	DOC, POC, SPM
Mackenzie Monitoring Program/ DUCCEM	mackenzie-monitoring.awi.de Morgenstern and Gottschalk, 2025	East Channel at Inuvik	2023-present; year round	Water samples	47	DOC, POC, SPM, a_{CDOM}^a

^aAbsorption of colored dissolved organic matter (a_{CDOM})

140 ^bParticulate absorption (a_P)

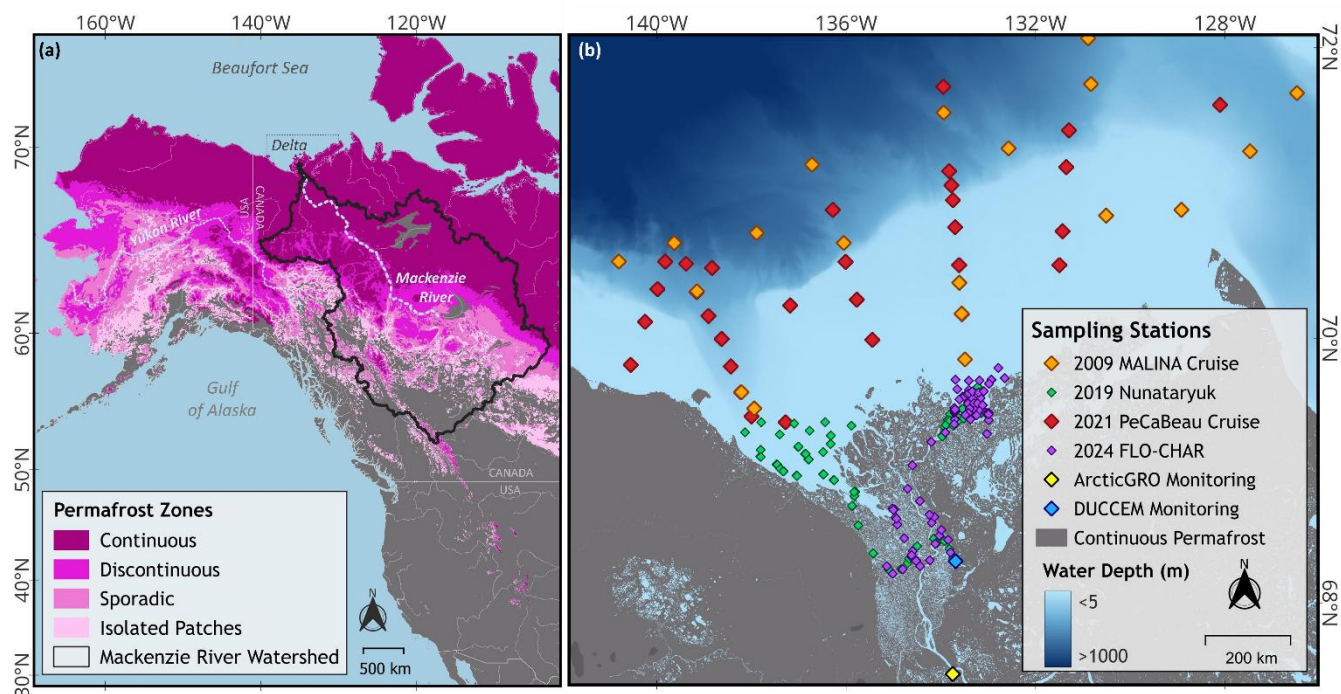


Figure 1. (a) The Mackenzie River watershed footprint with the extent of permafrost zones throughout as described in Brown et al. (2002) (b) all in-situ observations collected from 2009-2024 across the land-ocean transition of the Mackenzie River Delta-southern Beaufort Sea region with the different campaigns and respective year specified in the legend (Table 1).

150

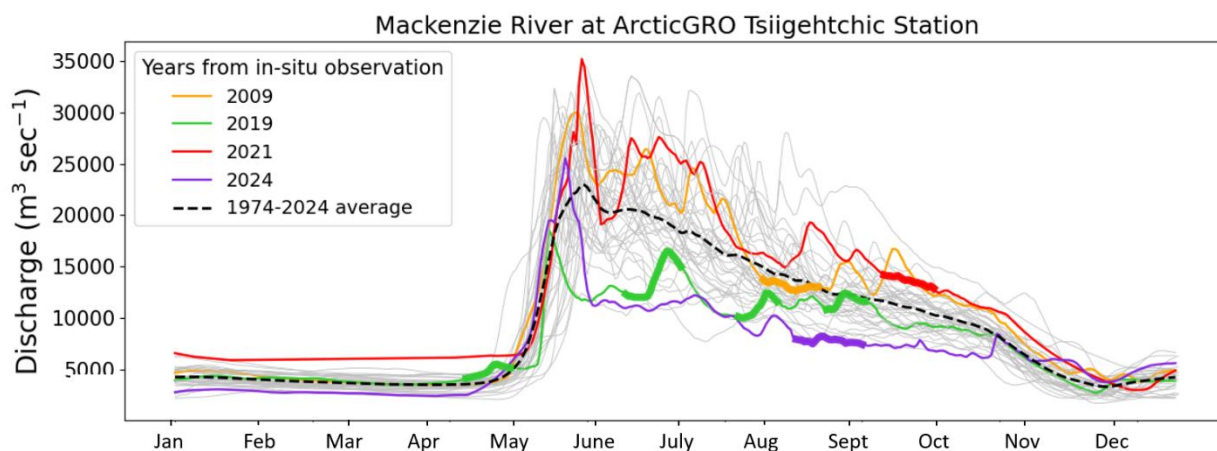


Figure 2. Mackenzie River discharge at the Arctic-Red River gauge station at Tsiigehtchic (ArcticGRO monitoring; yellow diamond in Figure 1b) from 1974 to 2024 (annual hydrograph). The annual average hydrograph for this period is indicated



155 with a black dashed line and the hydrographs for the four years in which in-situ sampling campaigns took place are indicated
by respective color with sampling periods indicated by a thicker line (Arctic Great Rivers Observatory, Absorbance Dataset,
Version 20250402. <https://www.arcticgreativers.org/data>).

2.2 Sample collection

During ship-based expeditions aboard the CCGS *Amundsen* (MALINA, PeCaBeau), water samples were taken using Niskin
160 bottles on a Rosette system at defined depths along predefined transects across the shelf. For land-based expeditions
(Nunataryuk, FLOCHAR, Mackenzie Monitoring), a combination of small draft boats, hovering helicopter, and riverbank
sampling were used to sample freshwater locations within the delta and the shallow receiving waters of the two main outflow
regions of the Mackenzie River: Kugmallit Bay to the east, and Shallow Bay and Mackenzie Bay to the west.

During land-based expeditions (Nunataryuk, FLOCHAR), discrete water samples were collected as close to the surface as
165 possible using a pump and plastic hose to fill 10 L containers. For the Mackenzie Monitoring program, river water was sampled
at the shore just below the water surface with 1 L bottles. The pump and sample containers were rinsed twice with sample
water prior to collection. All water samples were filtered within 12 hours of collection (see details on filtration below).

Since this study focuses on characterizing bio-optical relationships for satellite retrievals, only surface water samples (< 5 m
water depth; assuming a homogenous freshwater upper layer) were included in the compiled dataset. Details of each of the
170 aforementioned sampling techniques can be found in the following literature for each campaign (Masciotte et al., 2021; Lizotte
et al., 2023; Bröder et al., 2022; Morgenstern & Gottschalk, 2023).

2.3 Biogeochemical parameters

The following section describes the methods used to collect and analyze biogeochemical parameters presented in this study.
The methods for each parameter across individual campaigns and monitoring projects are slightly different. Differences
175 significant to this study are explained below, but for information beyond what is described, further methodological details on
these campaigns are provided in Massicotte et al. (2021), Broder et al. (2022), Lizotte et al. (2023) and Morgenstern and
Gottschalk, (2025).

For DOC, the MALINA and Nunataryuk, samples were filtered through 25 mm, Millipore Whatman GF/F pre-combusted
filters with a nominal pore size of 0.7 μm . For the FLOCHAR and Mackenzie Monitoring programs, 47 mm, 0.45 μm Millipore
180 cellulose acetate (CA) filters were used. Filtration setup varied slightly between each campaign. For the MALINA campaign,
water samples were gravity filtered from the Niskin bottles used for collection. For the Nunataryuk, PeCaBeau, and Mackenzie
Monitoring, 30 mL syringe filtration was used. A Nalgene filtration unit was used for FLOCHAR samples. All filtered samples
were acidified and stored frozen (-20°C) immediately after processing in pre-combusted borosilicate glass vials. DOC
concentrations were measured using a high-temperature catalytic oxidation (TOC-VCPH, Shimadzu) at the Alfred Wegener
185 Institute (AWI, Potsdam, Germany) (Benner and Strom, 1993). For ArcticGRO, samples were analyzed on a Shimadzu
TOC/TN analyzer at the Woodwell Climate Research Center (WHRC) in the United States.

Water samples for the analysis of colored dissolved organic matter absorption (a_{CDOM}) were filtered and measured using
slightly different procedures across the individual campaigns. For the Mackenzie Monitoring and FLOCHAR programs,



190 samples were filtered through 0.45- μm cellulose acetate (CA) syringe filters and subsequently analyzed at the German
Research Center for Geosciences (GFZ, Potsdam, Germany) using a PerkinElmer LAMBDA 950 UV-Vis spectrophotometer.
Sample processing and analytical protocols followed Juhls et al. (2021). Samples collected during the PeCaBeau, MALINA,
and Nunataryuk campaigns were filtered through 0.2- μm GHP syringe filters (Acrodisc Inc.) and analyzed with a Liquid
Waveguide UltraPath system (World Precision Instruments Inc.) immediately after sampling aboard ship (MALINA and
PeCaBeau) or following short transport to the laboratory (Nunataryuk). For ArcticGRO, absorbance was measured between
195 200-800 nm, at 1 nm intervals, using a Shimadzu UV-1800 spectrophotometer and a 1 cm pathlength.
Samples for POC from Nunataryuk and PeCaBeau, were filtered using pre-combusted 47-mm Millipore Whatman GF/F filters,
samples from FLOCHAR, Mackenzie Monitoring, and ArcticGRO used pre-combusted 25-mm Millipore Whatman GF/F
filters. For Nunataryuk, 0.25-1.6 L of sample volume was filtered while 2-10 L of sample volume were filtered for PeCaBeau,
and 5-6 different volumes of sample were filtered for each station ranging from 0.05-0.4 L for the FLOCHAR campaign. All
200 sample filters were dried at room temperature, 50° C, or freeze-dried. For Nunataryuk, samples were weighed three times each
with a Mettler Toledo microscale at Laval University (Quebec City, Canada). Two punched replicates from the filters were
placed into tin capsules and processed in a PerkinElmer elemental analyzer (PE 2400 Series-II CHNS/O Elemental Analyzer).
For Mackenzie Monitoring, POC content was measured using a punched portion of the GF/F filters, fumigated and dried while
analysis was completed on an Elemental Analyzer (EA) interface coupled to a stable isotope analyzer (Thermo Scientific EA
205 IsoLink IRMS System) using standards Ethylenediaminetetraacetic acid (EDTA, Sigma Aldrich), following (Lattaud et al.,
2025). For FLOCHAR, POC concentration was processed at Helmholtz-Zentrum Hereon (Geesthacht, Germany) where the
samples were acidified to remove carbonates, pressed in tin cups and the particulate carbon concentration determined in a
Vario TOCcube instrument (Elementar, Germany). For PeCaBeau, the sample filters were not washed for salts after filtration,
which may underestimate the resulting measurement, but we do not believe this has a significant impact.

210 For particulate absorption (a_p) samples from Nunataryuk, approximately 20-500 mL of water was filtered through 25-mm
Whatman GF/F pre-combusted filters. A spectrophotometer (Cary 100; Agilent Technologies, Inc.) equipped with a small
(60 mm) integrating sphere was used to measure the transmittance and reflectance from the sample filters (350 to 800 nm at 1-
nm increments) (Tassan & Ferrari, 1995; 2002). For PeCaBeau, water samples were filtered through pre-combusted 25-mm
Whatman GF/F filters. The filters were stored frozen until measurements of particulate absorption were made at Scripps
215 Institution of Oceanography (San Diego, California, USA) using a custom-made spectrophotometer attached with a 150 mm
integrating sphere. For FLOCHAR, one volume (3-30 mL) was filtered on a combusted 25-mm GF/F filter for samples
measured in the visible (350-800 nm) and one volume (100-400 mL) was filtered on a combusted 25-mm GF/F for samples
measured in the near infrared (NIR, 700 - 2500 nm). All sample filters were directly measured with a QFT-ICAM (Röttgers et
al., 2015). Here, measurements with a PSICAM (Röttgers & Doerffer, 2007) conducted on unfiltered and filtered water samples
220 (500 ml; 0.2 μm) are used for accurate a_p measurements in the wavelength range 400 - 700 nm, and finally combined with the
results of the QFT-ICAM.



For SPM samples from Nunataryuk and PeCaBeau, pre-combusted 47 mm Millipore Whatman GF/F filters were used, and pre-combusted 25-mm Millipore Whatman GF/F filters were used for FLOCHAR and Mackenzie Monitoring. For Nunataryuk, samples were weighed three times each with a Mettler Toledo microscale. For FLOCHAR, 5-6 different volumes of the same sample (0.1-2 L) were filtered using a Nalgene filtration unit as described in (Röttgers et al., 2014). For Nunataryuk and Mackenzie Monitoring, 30-mL syringe filtration was used. For all samples, values for SPM were obtained by subtracting the initial weight of the blank filters from the final weight of the dried particulate-matter-laden filter. For PeCaBeau, the sample filters were not washed for salts after filtration, which may underestimate the resulting measurement, but we do not believe this has a significant impact.

2.4 Optical parameters

Inherent optical properties (IOPs) such as light absorption, beam attenuation, and scattering coefficients, define apparent optical properties (AOPs), which include R_{rs} , which is often used synonymously with ocean color, are measured from water samples with benchtop spectral absorption and attenuation sensors (AC-s, WetLabs). The total light absorption ($a_t(\lambda)$) and attenuation ($c_t(\lambda)$) coefficients were measured by filling the optical path of the AC-s (10 cm) with the unfiltered water sample. The dissolved absorption and attenuation were measured using the filtered water sample, identical ones were used for UltraPath measurements (0.2 μm filter, GHP Acrodics). Ultra clean (Milli-Q) water was used as a reference. The absorption and scattering coefficients were determined by considering temperature and salinity effects (Pegau et al., 1997; Sullivan et al., 2006; Bröder et al., 2022). To relate water sample properties to radiometric measurements, absorption at 443 nm was analyzed alongside DOC and POC concentrations from co-located samples collected during all campaigns. This is a commonly used wavelength in ocean-color remote sensing due to its sensitivity to multiple optically active constituents and its widespread availability across satellite missions. Identifying and characterizing these variabilities is necessary to understand and define the limits of validity of these bio-optical relationships in order to best estimate DOC and POC across the fluvial-marine compartments. In order to evaluate the limitations of these relationships, we compared the relationship of each compartment (river, delta, coastal, marine) with a cross-compartment relationship that spans the full fluvial-marine and salinity gradient. For this study, filtration for particle absorption in the visible (350-800 nm) called for 2-20 mL of sample filtered through a combusted 25-mm GF/F filter. These filters were directly measured with a quantitative filter technique using an integrating cavity absorption meter (QFT-ICAM) as described in (Röttgers et al., 2015). Because this study synthesizes datasets collected during several independent campaigns between 2009 and 2024, minor methodological differences in sample collection, filtration, and analytical protocols exist among the contributing datasets. In particular, different filter types and pore sizes were used for dissolved measurements (0.7 μm GF/F filters during MALINA and Nunataryuk while 0.45 μm cellulose acetate filters were used during FLOCHAR and the Mackenzie Monitoring program). Additionally, CDOM absorption was measured using different optical systems (e.g., UltraPath/Liquid Waveguide systems versus conventional spectrophotometers). Such differences can potentially influence measured DOC concentrations and CDOM absorption by altering the operational definition of the dissolved fraction or by introducing small instrument-specific biases. However, previous methodological intercomparisons indicate that these effects are generally small relative to the natural variability observed across Arctic fluvial-



marine gradients. For example, filter comparison experiments in the Lena River showed that DOC concentrations measured with 0.45 μm and 0.7 μm filters differed on average by only $\sim 2.5\%$, while $a_{\text{CDOM}(443)}$ measurements obtained using different filtration approaches and analytical instruments typically varied by $\sim 5\text{--}10\%$ without showing a systematic bias (Supplementary Fig. S1 in Juhls et al., 2021). These differences are small compared with the large spatial gradients observed in this study. While such methodological variability may introduce minor scatter in cross-campaign comparisons and bio-optical regressions, it is unlikely to affect the major patterns or relationships identified across the fluvial-marine continuum. Nonetheless, the compilation of long-term multi-campaign datasets highlights the importance of continued efforts toward methodological harmonization in Arctic monitoring programs to further improve the comparability of optical and biogeochemical measurements.

2.5 Radiometric data

Radiometric measurements were conducted using a variety of instrument setups for both ship and land-based expeditions to capture the in-situ water reflectance spectra (R_{rs}). Table 2 provides detailed information on sampling techniques for each sampling campaign.

Table 2. Details of radiometric measurements made during each sampling campaign from 2009-2024.

Campaign	Instrument type	Deployment	Sensor type	Spectral range/resolution
MALINA 2009 (Massicotte et al., 2021)	Compact Optical Profiling System (C-OPS)	Profile	Downwelling irradiance (E_d) Upwelling radiance (L_u) Global solar irradiance (E_s)	320-780 nm @ specific wavelengths
Nunataryuk 2019 (Lizotte et al., 2023)	Compact Optical Profiling System (C-OPS)	Above-water Profile	Downwelling incident irradiance (E_s) Downwelling irradiance (E_d) Upwelling radiance (L_u)	395-865 nm @ specific wavelengths 395-865 nm @ specific wavelengths
PeCaBeau 2021 (Broder et al., 2022)	TriOS Ramses	Above-water	Downwelling radiance (L_{sky}) Upwelling radiance (L_u) Downwelling irradiance (E_d)	300-850 nm @ 4 nm increments
	TriOS Ramses	Floating	Upwelling radiance (L_u)	300-850 nm @ 4 nm increments
	TriOS Ramses	In-water	Upwelling radiance (L_u), 2x Downwelling irradiance (E_d)	300-850 nm @ 4 nm increments
FLOCHAR 2024	TriOS Ramses	Above-water	Downwelling radiance (L_{sky}) Upwelling radiance (L_u), 2x Downwelling irradiance (E_d)	350-950 nm @ 2.5 nm increments
	TriOS Ramses	Floating	Upwelling radiance (L_u)	350-950 nm @ 2.5 nm increments
	TriOS Ramses	Profile	Downwelling irradiance (E_d)	



			Upwelling radiance (L_u) Downwelling irradiance (E_d)	350-950 nm @ 2.5 nm increments
--	--	--	--	--------------------------------

270

2.6 Optical Water Type (OWT) classification

In situ measurements of bio-optical properties are essential for the calibration and validation of OCRS algorithms. When integrated with radiometric observations (e.g., upwelling radiance, downwelling irradiance, and water-leaving reflectance), these measurements provide critical ground-truth data to improve satellite-derived estimates of POC and DOC concentrations.

275 For further interpretation of these bio-optical and radiometric measurements, we employed the OWT classification scheme by Bi and Hieronymi (2024). This method distinguishes clusters of R_{rs} , which are determined by different concentration ranges of the optically active water constituents. The classification scheme aims to a broad applicability for inland, coastal, and ocean

280 waters, as well as for various hyper- and multispectral band settings of in situ measurement methods and satellite missions. In this method, three optical variables are extracted from the R_{rs} spectrum to classify the OWT, leveraging both the spectral shape and magnitude. These are: the apparent visible wavelength (AVW) between 400 and 800 nm, the (Box-Cox-transformed) spectral area below three red, green, and blue bands (A_{BC}), and the normalized difference index at green and red (NDI). Ten types are defined, covering the optical extremes from oligotrophic ocean waters (OWT 1), to eutrophic waters with high phytoplankton biomass (OWT 5), and to CDOM-rich waters (OWT 7). OWT labels ending with ‘a’ and ‘b’ are intended for types with similar spectral shapes but different magnitudes, with ‘b’ generally representing a variant with higher brightness.

285 In color scales, OWT 1 and 2 stand for blue, 3 for turquoise, 4 and 5 for greenish, 6 for light brown and 7 for dark brown waters. For the purposes of this study and to better represent the regional optical variability, broader categories river, delta, coastal, and marine are used as well.

2.7 Hydro-salinity Compartment Delineation

To examine the fate and variability of biogeochemical parameters across the fluvial-marine transition of the Mackenzie River Delta-Beaufort Sea system, we generated a large dataset that covers spring freshet to late summer for years between 2009 and 290 2024 (Table 1, Fig. 1 and 2). Compared to previously published studies, this synthesis presents a unique compilation of riverine, deltaic distributary, coastal and marine water types, which we use to examine biogeochemical relationships and calculate flux of organic matter across the land-sea transition.

The compiled dataset was first classified into three water types according to in-situ salinity measurements (CastAway CTD) 295 based on the Venice System (1958): freshwater (salinity <0.5 psu), coastal (0.5-20.0 psu), and marine (>20 psu). To further examine the variability within the dynamic delta zone of the Mackenzie River Delta, we subclassified freshwater based on channel morphology: main river channel (river compartment) upstream of the distributary network channels (delta compartment) (Fig. 1b). The river compartment includes the main stem of the Mackenzie River channel before bifurcation downstream of Tsigethchiic to distributary channels at ~150 km from the river mouth (Tarasenko et al., 2023). The delta 300 compartment includes distributary channels downstream of the first major bifurcation upstream of the floodplain, where interaction between the river and deltaic channels occurs until the coastal waters.



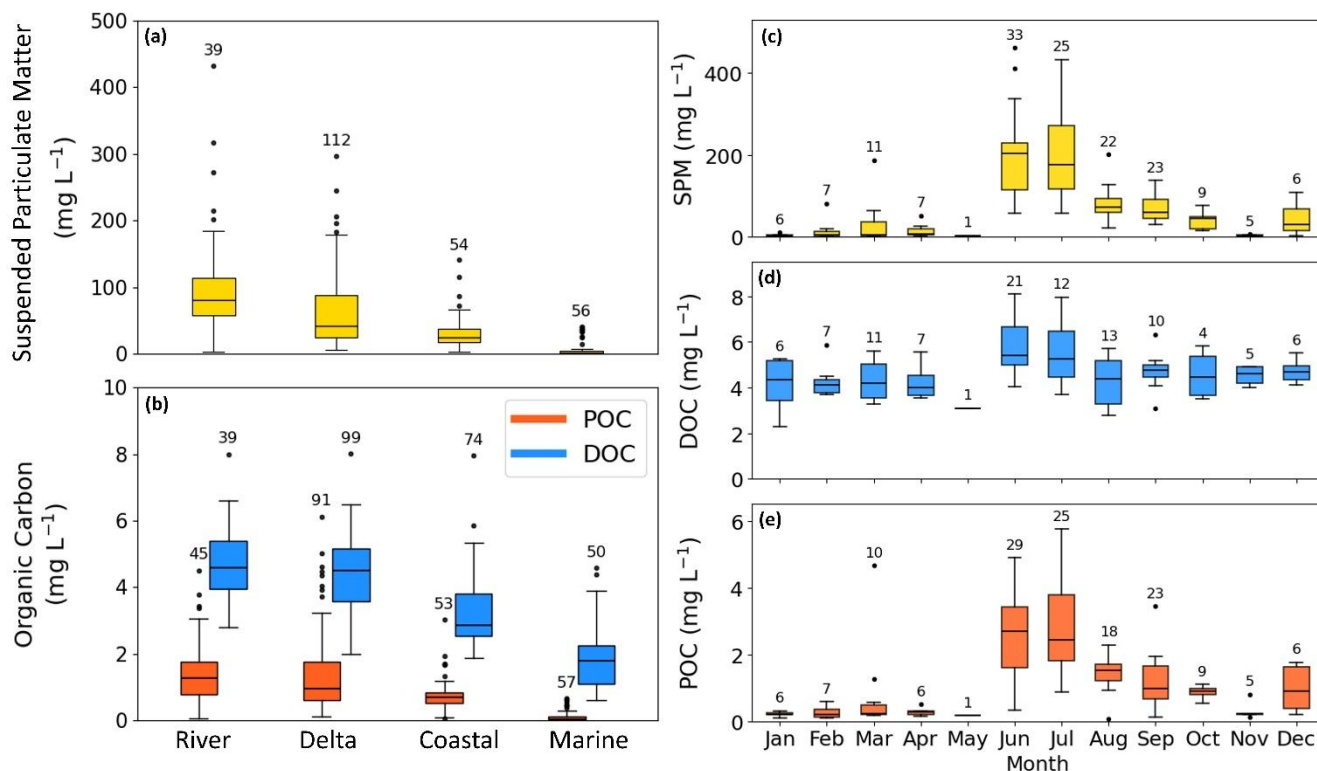
3. Results

3.1 Spatial variability of DOC, POC, and SPM

305 The four aquatic compartments classified by salinity and channel morphology are used in this study to describe the spatial patterns of DOC, POC, and SPM across the fluvial-marine transition. The freshwater main river channel is hereafter referred to as the “river” compartment, freshwater distributary channels of the deltaic floodplain as the “delta” compartment, waters with salinity 0.5-20.0 psu as the “coastal” compartment, and waters >20.0 psu as the “marine” compartment. Sampling coverage was not evenly distributed across seasons or compartments, reflecting the multi-campaign nature of the compiled dataset.

310 The distribution of DOC, POC, and SPM concentrations was examined using all available data throughout the campaign years (2009-2024) and the two monitoring stations. DOC concentrations were highest in the river compartment ($n=39$; mean $4.78 \pm 1.12 \text{ mg L}^{-1}$) and exhibits a steady decline across the fluvial-marine gradient towards marine waters ($n=50$; mean $1.88 \pm 0.96 \text{ mg L}^{-1}$; Fig. 3a). POC exhibited a broadly similar decrease along the gradient but showed greater variability within the delta compartment ($n=91$; mean $1.38 \pm 1.21 \text{ mg L}^{-1}$) compared to the river compartment ($n=45$; mean $1.49 \pm 1.06 \text{ mg L}^{-1}$). Similarly, 315 SPM concentrations were highest in the river compartment ($n=39$; mean $104.63 \pm 86.20 \text{ mg L}^{-1}$) and decreased markedly towards marine waters ($n=56$; mean $7.17 \pm 12.44 \text{ mg L}^{-1}$; Fig. 3) with the largest variability observed in river and delta waters. Sample availability varied among compartments and seasons, reflecting differences in campaign focus and accessibility across the fluvial–marine transition.

Examining the seasonality of the river compartment, where year-round observations are available from the ArcticGRO 320 monitoring station at Tsiigehtchic, SPM and POC concentrations show peaks during the freshet (May-June) and remain elevated into summer (August-September). A second, smaller and more variable peak occurs during the late summer/fall (September-October) (Fig. 3c&d). DOC concentrations exhibit a similar summer maximum, followed by increased concentrations during autumn and early winter (October-December) (Fig. 3e).



325

Figure 3. Spatial variation of biogeochemical parameters (a-b) across the river, delta, coastal and marine compartments of the fluvial-marine transition zone from all campaign data from 2009-2024 and (c-e) monthly average concentrations in the river compartment from ArcticGRO year-round observations at Tsiigehtchic from 2009-2024. Boxplots show median, quartiles, outliers and range for measurements of SPM (yellow), DOC (blue), and POC (orange). The river compartment is delineated as the freshwater main river channel of the Mackenzie River, the delta compartment defined as the freshwater distributary channels of the deltaic floodplain, waters with salinity 0.5-20.0 psu are defined as the “coastal” compartment, and waters >20.0 psu are defined as the “marine” compartment.

Concentrations of dissolved and particulate constituents decreased markedly with increasing salinity across the salinity gradient along the fluvial-marine transition (Fig. 4). DOC exhibited a strong negative linear relationship with salinity (0.2-35 psu) ($R^2=0.82$), with highest concentrations (>10 mg L⁻¹) occurring at very low salinities and declining to <1 mg L⁻¹ at salinities above 30 psu (Fig. 4a). Fig. 4b depicts $a_{CDOM}(443)$ showing a similar inverse relationship with salinity (0.2-35 psu) ($R^2=0.74$), with values decreasing from >4 m⁻¹ in freshwater to near-zero in marine waters. POC and SPM concentrations also generally declined with increasing salinity, although with greater scatter relative to dissolved components. POC concentrations were highest at low salinities (>5 mg L⁻¹) and decreased toward near-zero values in marine waters (Fig. 4c). Similarly, SPM concentrations were highest in the freshwater endmember (up to 250 mg L⁻¹) and declined substantially along the salinity

340

gradient, with most marine samples exhibiting concentrations below 20 mg L⁻¹ (Fig. 4d). Overall, these relationships demonstrate pronounced decreases in both dissolved and particulate organic matter pools along the fluvial–marine mixing continuum.

345

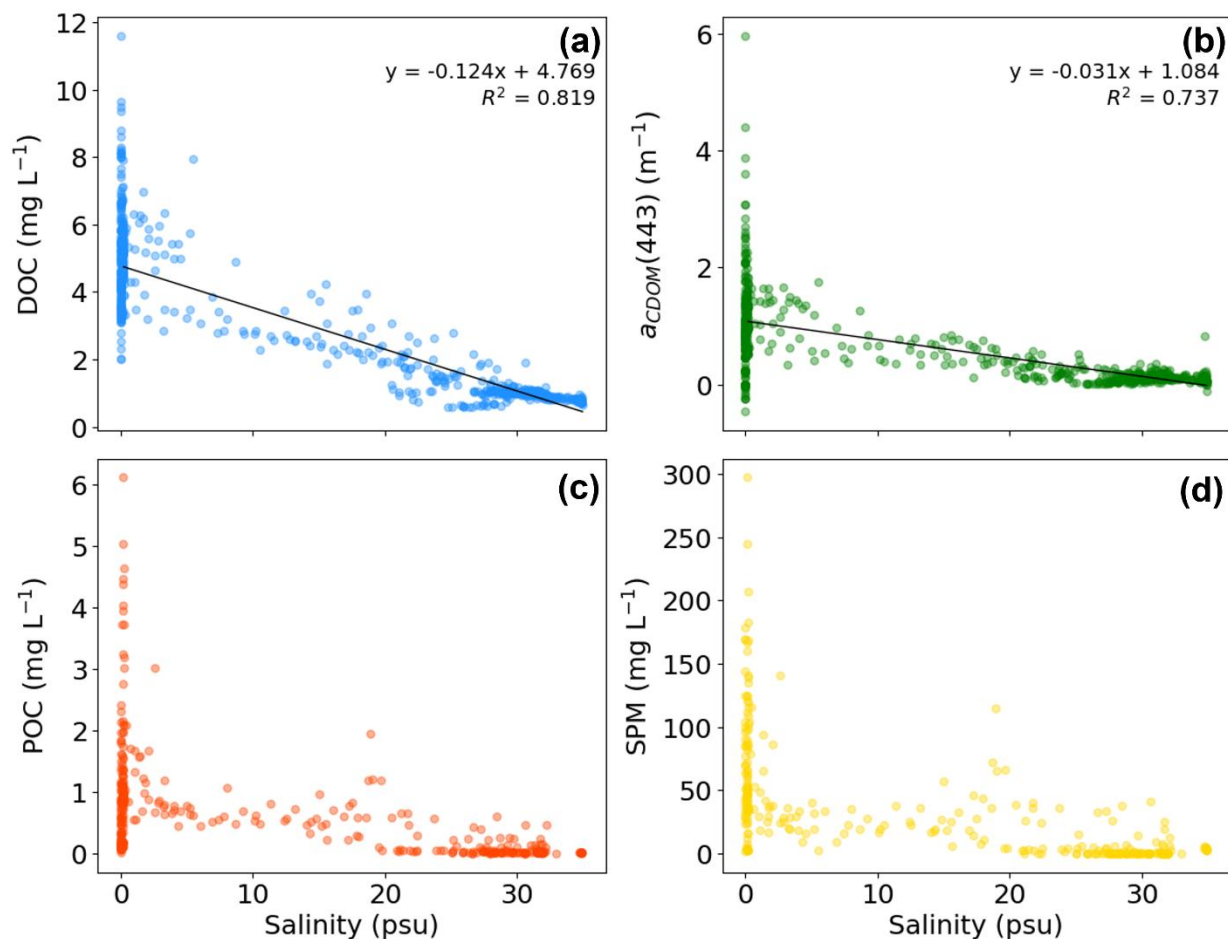


Figure 4. Linear regressions between salinity (psu) and (a) DOC, (b) $a_{CDOM}(443)$, (c) POC and (d) SPM across the fluvial-marine salinity gradient from all campaign data from 2009-2024. The solid black lines represent the regression. The regression analysis filtered out observations for salinity <0.2 psu for all four parameters. Equations and coefficients of determination (R^2) are shown for (a-b).

350

Across the salinity gradient, total OC concentrations declined from freshwater to marine environments (Fig. 5a). This decrease was primarily driven by a reduction in the dissolved fraction of OC, which constituted the predominant fraction throughout the fluvial-marine gradient, while POC contributed a smaller and more variable fraction. The most pronounced reduction in total OC occurred at low salinities (<10 psu), followed by a more gradual decline towards marine waters. Variability was



355 highest at low salinity, where both DOC and POC showed a broader range of concentrations, whereas offshore waters showed
lower concentrations with reduced variability. When aggregated by compartment (Fig. 5b), the river and the delta
compartments exhibited the highest total OC concentrations, with DOC consistently exceeding POC, while the marine
compartments showed the lowest total OC and the smallest relative POC contribution to the OC pool. Note that sample numbers
varied among salinity bins and compartments, reflecting uneven spatial and seasonal sampling coverage across the fluvial-
360 marine transition.

3.2 Associated optical properties and absorption characteristics

Comparison of particulate and dissolved absorption from filtered and unfiltered water samples revealed clear differences along
the fluvial-marine continuum. Particulate absorption (a_p) consistently dominated over the dissolved component (a_{CDOM}) along
365 the salinity gradient (Fig. 5c), with a distinct decrease in a_p above 20 psu. In contrast, a_{CDOM} exhibited a more gradual decline
and showed less variability than a_p . A comparable pattern is evident across the freshwater-to-marine compartments (Fig. 5d).
While a_{CDOM} remains relatively stable from the river to the coastal compartment, a_p demonstrates a progressive decline across
this transition. In the marine compartment, located furthest from the influence of the sediment plume, both particulate and
dissolved absorption components show a marked decrease. Overall, these patterns indicate a systematic shift in the relative
370 contributions of particulate and dissolved optical components along the fluvial-marine continuum. While dissolved organic
carbon constituted the dominant fraction of total organic carbon, particulate absorption (a_p) contributed disproportionately to
total absorption, indicating that particulate components exert a stronger influence on optical properties than suggested by their
relative contribution to total organic carbon concentrations.

3.3 Optical water types

375 The distribution of optical water types (OWTs) classified by maximum membership shows a systematic shift along the salinity
gradient. The distribution of optical water types (OWTs) with maximum membership shows a systematic shift along the salinity gradient
and across fluvial-marine compartments (Fig. 5e–f). At low to medium salinities (0–20 psu), OWT 6 represents the dominant
class, it stands for bright brown water with a high concentration of detritus. In addition, classes 5a and 5b contribute with a
green and bright green appearance and a much lower sediment proportion. With increasing salinity, the relative contribution
380 of OWT 5a and 5b increases and becomes more prevalent within the coastal salinity range. At salinities exceeding 20 psu, the
sediment component decreases substantially, while classes defined for transitional waters OWT 3a and OWT 2 increase in
relative abundance. When grouped by compartment (Fig. 5f), delta samples are primarily associated with OWT 6, whereas
coastal waters show a broader distribution of OWT memberships, including a few cases characterized by higher phytoplankton
biomass OWT 5a and 5b. The marine compartment is characterized by a shift toward OWT 3a and OWT 2, with only minor
385 contributions from higher-numbered OWT classes. Overall, the distribution of OWT memberships indicates a gradual
transition in optical regimes across the fluvial–marine continuum.

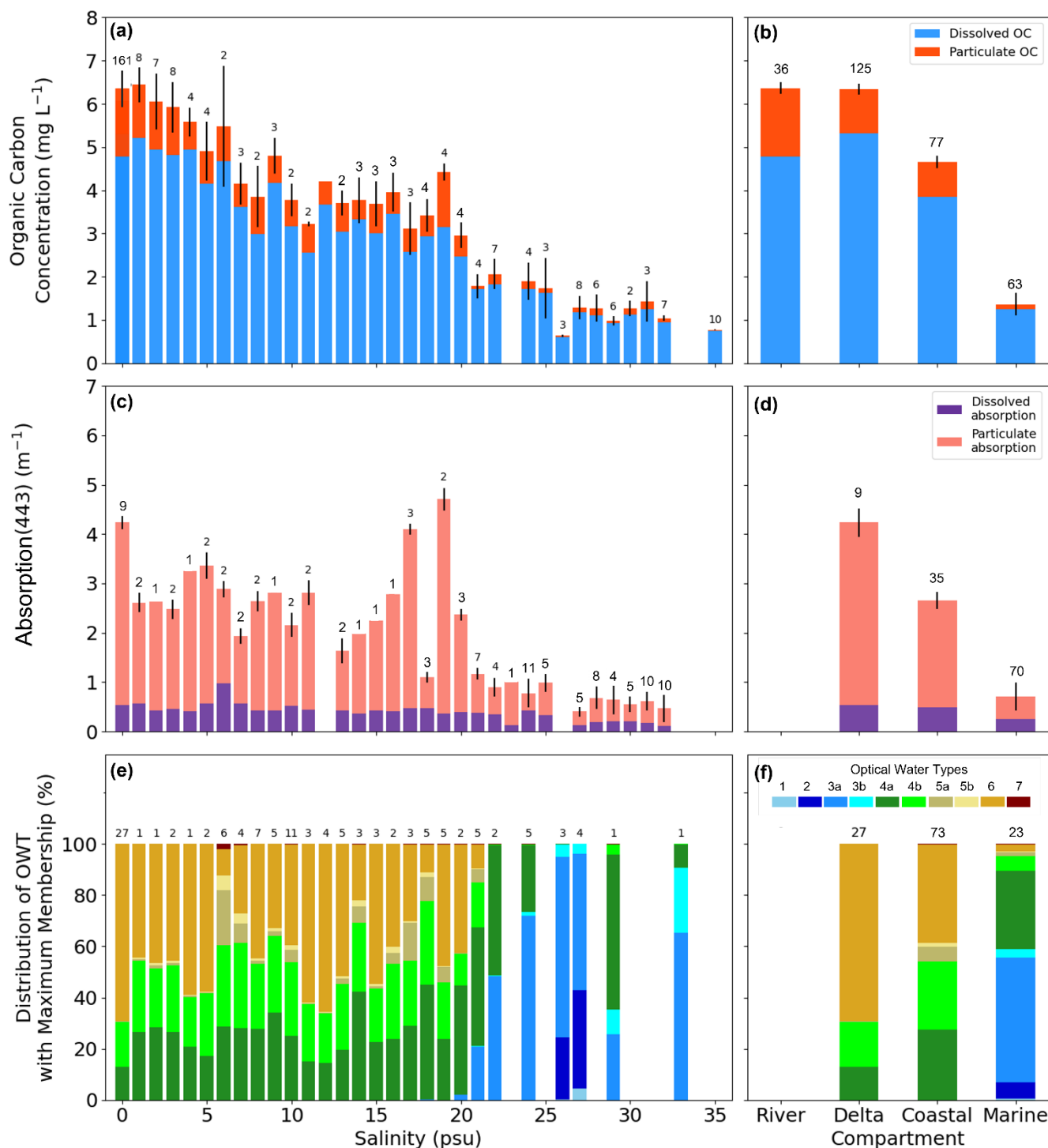


Fig. 5. (a) Changes in DOC (blue) and POC (red) concentration along the salinity gradient and (b) from river to delta to coastal to marine compartments for samples collected during the open-water season from the MALINA, Nunataryuk, PeCaBeau,



FLOCHAR, ArcticGRO, and Mackenzie Monitoring campaigns during 2009-2024. The middle graphs (**c**, **d**) show the relative contributions to the light absorption coefficient of dissolved (purple) and particulate (pink) components from MALINA, Nunataryuk, PeCaBeau, and FLOCHAR campaign samples. The lower graphs (**e**, **f**) show the contributions of OWT memberships along the salinity gradient and along the freshwater-marine compartments from a subset of data where both radiometric and optical data was available. Error bars represent standard error and the numbers above bars reflect the number of samples.

3.4 Bio-optical relationships

A strong, non-linear relationship was found between observed DOC concentrations and $a_{CDOM(443)}$ across the full salinity gradient, with an overall coefficient of determination of $r^2=0.81$ (Fig. 6a). While compartment-specific relationships were generally linear, combining samples across compartments resulted in a non-linear relationship. The overall regression reflects the combined variability of river and delta samples at higher $a_{CDOM(443)}$ values, while marine samples form a tightly clustered low-concentration group. The strength and type of this relationship vary markedly among compartments with the coastal compartment exhibiting the strongest linear relationship ($r^2=0.86$), whereas the delta ($r^2=0.54$) and marine ($r^2=0.49$) compartments showed weaker relationships and narrower range of DOC variability. The compartment-specific regressions differed not only in strength but also in slope, with steeper relationships observed in coastal and marine compartments compared to river and delta samples, contributing to the non-linear cross-compartment scaling.

A linear pattern is observed between POC and $a_P(443)$ across delta, coastal, and marine compartments (Fig. 6b), with an overall $r^2=0.73$. Note, that no $a_P(443)$ data was available for the river compartment. Among individual compartments, the marine zone showed the strongest POC- $a_P(443)$ relationship ($r^2=0.81$), while the coastal compartment exhibited the weakest correlation ($r^2=0.59$). In contrast, the delta compartment shows a moderate relationship ($r^2=0.65$), indicating spatial variability in the optical-biogeochemical coupling of particulate matter. Slopes of the POC- $a_P(443)$ relationships were more consistent across compartments, resulting in a broadly linear cross-compartment relationship despite differences in correlation strength.

Samples associated with lower-numbered OWT classes clustered toward lower $a_{CDOM(443)}$ and $a_P(443)$ values, whereas higher-numbered OWTs occupied the high-absorption end of the regression space within the subset of samples with available radiometric measurements (Fig. A1). Consistent with the observed POC- $a_P(443)$ relationships, POC concentrations exhibited a strong positive linear association with suspended particulate matter (SPM) across the dataset (Fig. A1; $r^2 = 0.69$, $n = 162$). POC increased linearly with SPM, with variability primarily driven by particle load (Fig. A1).

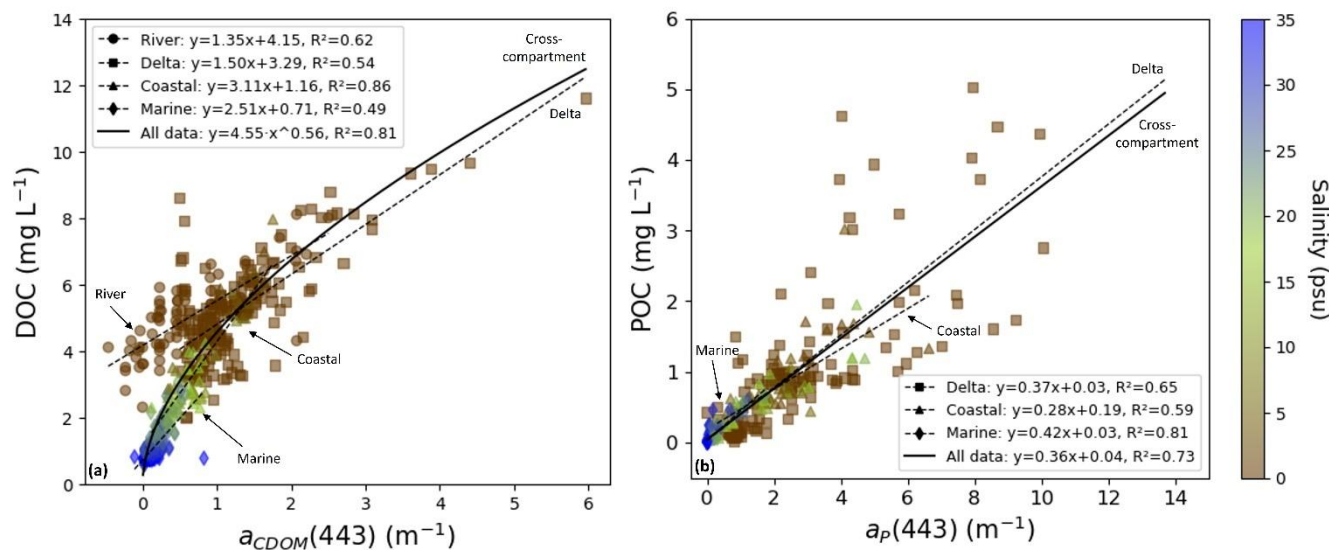


Fig. 6. Bio-optical relationships for measured in-situ (a) DOC and $a_{CDOM}(443)$ and (b) POC and $a_P(443)$ along the freshwater-marine salinity gradient during 2009-2024. The black solid line shows the regression of all samples (Massicotte et al., 2021, Lizotte et al., 2023, Bröder et al., 2022, this study, mackenzie-monitoring.awi.de) across all compartments. The dashed black lines show the relationship per compartment.

4. Discussion

4.1 Sediment and organic carbon processing across the land-ocean continuum

As freshwater riverine flow transits the interconnected network of distributary channels and moves towards the shallow coastal zone and eventually to the marine waters of the Beaufort Sea, biogeochemical processes modify the quality and quantity of OC and sediments along the transition through the fluvial-marine compartments, as reflected by the spatial gradients in DOC, POC and SPM observed across compartments (Fig. 3). Our observations indicate a progressive modification of both the quantity and quality of organic carbon along this continuum, suggesting active chemical and mechanical processing during transport through the deltaic network and nearshore plume. These processes include flocculation, photochemical and microbial degradation, remineralization and oxidation, which regulate the fate of terrigenous material during mixing with saline waters (Hernes & Benner, 2003; Vonk et al., 2015; Mann et al., 2016; Clark et al., 2022; Bertin et al., 2022). Similar spatial gradients in DOC, POC and SPM across riverine, deltaic and shelf environments have been documented for the Mackenzie system and other Arctic deltas, highlighting the role of distributary networks and shallow estuarine environments as active biogeochemical filters that modulate terrestrial carbon export prior to its delivery to the Arctic Ocean (Emmertson et al., 2008; Clark et al., 2022).

At the land-sea interface, where freshwater from the river and delta mixes with saline waters, our observations reveal abrupt shifts in DOC, POC, and SPM distributions, highlighting the mixing zone as a hotspot of material transformation (Fig. 3, 4). The strong decline in particulate loads and concurrent reorganization of DOC patterns across the plume suggest enhanced



440 aggregation, settling, and selective removal of terrigenous material during early stages of marine exposure. The mixing of
riverine freshwater with higher-salinity coastal waters enhances ionic strength and promotes flocculation and aggregation of
dissolved and colloidal organic matter, facilitating a transfer from dissolved to particulate organic carbon and enhancing
particle settling. The sharp decrease in POC from the delta to coastal compartment (~46 %; Fig. 3) is consistent with processes
such as flocculation and particle removal. Such aggregation-driven phase shifts are well documented in estuarine mixing zones
445 and contribute to the redistribution and removal of terrestrial organic matter within nearshore plume environments (Sholkovitz,
1976; Keil et al., 1997; Burd & Jackson, 2009; Clark et al., 2022). Simultaneously, as turbidity decreases from the river channel
mouth, sunlight (UV and visible light) interacts with the surface water, leading to a breakdown of particulate and dissolved
OC via photochemical degradation and oxidation and remineralization, likely reflected by the 28 % decrease in DOC as waters
reach the coastal compartment and an additional 15 % decrease in the marine compartment. These estimates are comparable
450 to those reported by (Bertin et al., 2025), who suggested that flocculation may account for up to 45 % of DOC loss.
The shallow distributary channels of deltas are typically characterized as areas of sedimentation and deposition. Here, this is
reflected by the 38 % decrease in SPM across the river to delta transition (Fig. 3). The much smaller decrease in POC (7 %)
and DOC (7 %) across these two compartments highlights the preferential deposition and retainment of mineral
sediments relative to organic particulates. While some transformation of OC is likely occurring in the delta compartment,
455 these patterns emphasize the dual role of the delta as both a site of retention and transformation. Despite DOC representing the
dominant fraction of OC, particulate material exerted a strong influence on optical absorption (Fig. 5c-d), indicating that
particle-driven processes shape the optical properties in near-delta environments. This reflects differences in specific
absorption efficiency, as suspended mineral and detrital particles exhibit higher absorption and scattering cross-sections than
dissolved organic matter (Doxaran et al., 2012). Processes such as primary production and in situ POC generation via
460 phytoplankton growth may also occur in deltaic waters, although are likely limited in these highly turbid waters due to reduced
light penetration (Clark et al., 2022).
Similar to the Yukon River Delta and Lena River Delta systems (Juhls et al., 2019; Clark et al., 2022), DOC concentrations in
the Mackenzie River Delta exhibited a distinct spring freshet peak (Fig. 2), followed by moderately elevated levels that
persisted through the ice free- season. This pattern suggests that snow-and ice-melt-driven inputs during breakup provide an
465 initial DOC pulse, while continued mobilization from catchment soils and small tributaries sustain concentrations into summer.
In contrast, POC and SPM showed more episodic variability, with significantly high freshet peaks followed by secondary
peaks during mid-summer high-discharge events (Fig. 3c & e; A1a & c). These dynamics highlight the combined influence of
seasonal hydrology and local deltaic processes or catchment disturbance processes, such as permafrost thaw bank erosion and
thermokarst lake dynamics (Douglas et al., 2023).
470 Salinity-DOC and salinity- $a_{\text{CDOM}(443)}$ relationships reveal a narrow zone of non-conservative behavior at low salinities (0–5
psu), where DOC concentrations decline more steeply than predicted by conservative mixing. This pattern is consistent with
partial transformation or removal of chromophoric DOM during the initial freshwater-marine transition. At salinities above 5
psu, both DOC and $a_{\text{CDOM}(443)}$ decrease linearly with salinity indicating predominantly conservative transport through the



inner plume, in agreement with Juhls et al. (2022) (Fig. 4a,c). The observed decline in $a_{CDOM(443)}$ from 3.2 to 1.8 m^{-1} within
 475 0–5 psu likely reflects a combination of processes and compositional shifts in DOM. Overall, these results indicate that most
 terrigenous DOC is transported conservatively through the inner plume, while a measurable fraction is altered or removed near
 the freshwater-marine interface. In contrast, POC and SPM both exhibited a strong decrease at low salinities, indicating distinct
 non-conservative behavior associated with particle settling (Fig. 4). The variation observed in particulate concentrations near
 15 psu could be reflective of resuspension and redistribution processes that can occur during offshore transport.

480 These transformations can have implications for air–sea CO_2 exchange. Terrestrial OC fluxes strongly influence CO_2 exchange
 in coastal waters (Nielsen et al., 2024). Recent estimates suggest that OC inputs reduce the AO’s net CO_2 sink strength by 7–
 14 % (Nielsen et al., 2022) and may convert some shelves into net CO_2 sources (Bertin et al., 2023). Our observations indicate
 non-conservative behavior and partial removal of DOC within the near-delta plume, deviating from a linear mixing line
 between freshwater and saline endmembers, suggesting that roughly 27 % of riverine DOC may be transformed or lost at low-
 485 salinity coastal waters. Scaling this first-order estimate to the mean Mackenzie River DOC export (~ 1.4 Tg C yr^{-1} ; Matsuoka
 et al., 2022) implies a potential removal of ~ 0.38 Tg C yr^{-1} within the mixing zone. Assuming a fraction of 10–15 % of this
 removed DOC undergoes photochemical mineralization (Bertin et al., 2023), this corresponds to an estimated CO_2 release of
 0.04–0.06 Tg C yr^{-1} . While approximate, these values underscore that DOC transformation in the low-salinity plume can
 represent a measurable contribution to coastal carbon outgassing.

490 The compartmental framework applied here provides a system-scale context for interpreting OC and sediment transport and
 retention across the Arctic land–ocean continuum (Fig. 7). The river, delta, coastal, and marine compartments reveal distinct
 regimes of organic carbon processing, reflected in the observed gradients in concentration, optical properties and bio-optical
 relationships (Fig. 3-6). By resolving these four distinct compartments across the entire salinity gradient, our results highlight
 how hydrodynamic sorting, mixing behaviors and optical regime shifts collectively shape OC dynamics in Arctic river-shelf
 495 environments. While similar patterns have been reported in other observations from Arctic river–shelf systems (Juhls et al.,
 2019; 2020; Clark et al., 2022), here they are resolved consistently across all major components of the fluvial–marine
 continuum.

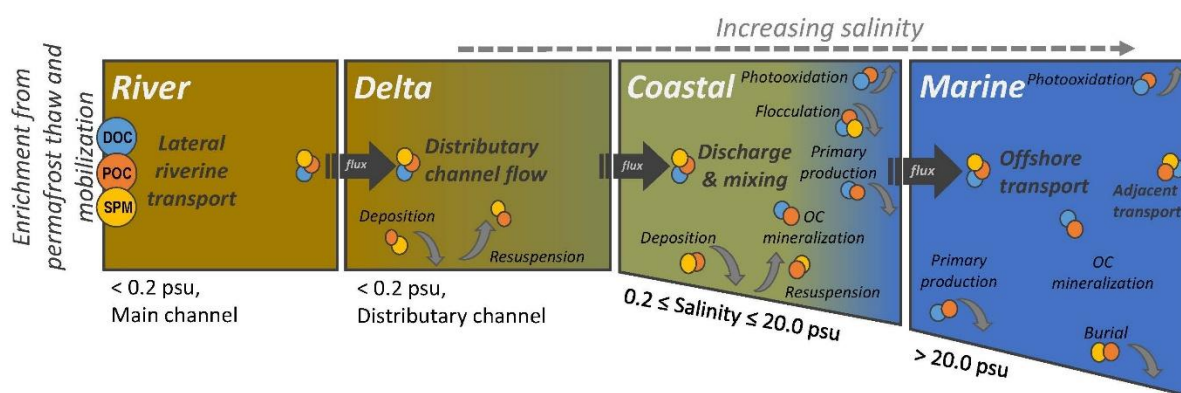




Fig. 7. Conceptual diagram demonstrating compartments along the fluvial-marine gradient in the Mackenzie River Delta-southern Beaufort Sea, delineated by salinity and channel size. Processes assumed to change concentrations of dissolved and particulate organic carbon and suspended particulate matter in the water column are indicated.

4.2 Bio-optical properties, OWT classification, and implications for remote sensing

To address uncertainties in satellite retrievals for optically complex Arctic coastal waters, we derived compartment-specific and cross-compartment bio-optical relationships spanning the full salinity gradient (Fig. 6). Within individual compartments, $\text{DOC}-a_{\text{CDOM}}(443)$ relationships were largely linear, whereas combining data across compartments resulted in a distinctly non-linear relationship. Similarly, $\text{POC}-a_p(443)$ relationships varied among compartments, reflecting differences in particle composition and optical regime along the continuum. These contrasts underscore that riverine, deltaic, coastal, and marine waters exhibit distinct optical and biogeochemical coupling, emphasizing the need for retrieval approaches that account for spatial variability rather than relying on a single pan-arctic parameterization.

When examined across the full dataset, the non-linear $\text{DOC}-a_{\text{CDOM}}(443)$ relationship (Fig. 6a) reflects systematic changes in the composition and optical quality of DOM along the fluvial-marine continuum. In the deltaic and low-salinity coastal zones, mixing of terrestrially derived, highly absorbing DOM with less colored marine DOM reduces CDOM absorption relative to DOC concentrations, flattening the relationship. Photobleaching and microbial processing during offshore transport preferentially remove chromophoric components relative to the total DOC (Cory et al., 2013). As a result, relationships that appear linear within individual compartments as reported in many studies (e.g., Mann et al., 2012; Walker et al., 2013, Novak et al., 2022) diverge non-linear when considered across the full cross-compartment continuum (Fig. 6a; black solid line) that integrates these compositional and optical shifts. While compartment-specific bio-optical relationships have commonly been used for regional retrievals (Doxaran et al., 2015; Matsuoka et al., 2013; 2017), our analysis shows that such relationships may not be transferable across the full salinity gradient. The emergence of non-linear cross-compartment behavior and changing slopes of the relationships with adding compartments (Fig. 6) suggests that synoptic-scale remote sensing requires relationships derived across the entire continuum of optical conditions.

Seasonal contrasts between the ice-free period and the full annual dataset further refine these patterns. Cross-compartment relationships between $\text{DOC}-a_{\text{CDOM}}(443)$ strengthened during the ice-free season (filtering data to only July–October), with the coefficient of determination increasing to $r^2=0.92$, whereas the $\text{POC}-a_p(443)$ relationship remained comparatively stable from $r^2=0.73$ annually to $r^2=0.72$ in the ice-free season (Fig. 6). Stronger coupling during the ice-free season likely reflects more consistent optical regimes, whereas winter freshwater samples add variability. Winter in situ observations were largely limited to freshwater compartments, as sea-ice cover restricted access to coastal and marine compartments. The spring freshet (May–June) represents an important but under sampled period in this seasonal cycle, when large pulses of freshwater transport elevated OC and sediment concentrations into the system. Although overall seasonal differences in bio-optical relationships were modest, continued monitoring remains essential, as Arctic warming and hydrological intensification are expected to increase variability in the amount and composition of CDOM and suspended particulates (Novak et al., 2022; Bertin et al., 2022, Chalov et al., 2023).



Our observations confirm that optical properties in Arctic coastal waters are strongly controlled by both CDOM and suspended particles, with their relative importance varying among compartments (Fig. 5c-d). The enhanced absorption in blue wavelengths (400–500 nm) produces the characteristic brown–green coloration of deltaic and nearshore waters. In low-salinity deltaic waters, a_P exceeded a_{CDOM} by a factor of ~ 1.5 –2, indicating that mineral and detrital particles dominate light attenuation despite DOC representing the major fraction of OC. This reflects differences in mass-specific absorption and scattering efficiency. These shifts illustrate how optical–biogeochemical coupling evolves across the fluvial–marine continuum, where particle-rich waters obscure CDOM signals and complicate retrievals of DOC from remote sensing. Photodegradation and compositional changes in CDOM further modulate these gradients (Grunert et al., 2021; Moran et al., 2022; Ward et al., 2017; Clark et al., 2022), underscoring the need for cross-compartment, or OWT-specific bio-optical algorithms (Fig. A2) in Arctic coastal and deltaic environments.

While bio-optical relationships refine the retrieval of DOC and POC, optical water type (OWT) classification provides an additional framework for interpreting optical variability and guiding algorithm selection in Arctic coastal waters. In our dataset, OWT distributions revealed a structured transition from OWT 6 dominance in river and delta compartments toward increased contributions of OWT 4a–4b in coastal waters and OWT 3a–2 in marine environments (Fig. 5f). Previous studies have associated higher-numbered OWT classes with stronger particulate and detrital scattering signatures, whereas lower-numbered classes typically reflect increasing contributions of phytoplankton and clearer water optical conditions (Bi and Hieronymi, 2024). The observed progression therefore suggests a shift from particle-rich delta waters toward optically clearer offshore regimes, consistent with the measured changes in a_P and a_{CDOM} along the fluvial–marine continuum.

Within the delta compartment, localized occurrences of OWT 4a and 4b likely reflect reduced hydrodynamic connectivity and enhanced particle settling in smaller distributary channels and floodplain environments. Such conditions may promote changes in the relative contributions of detrital material, phytoplankton biomass, and CDOM, resulting in optical regimes that differ from those of the main plume pathway. By linking reflectance-based OWT classes to dominant optical regimes, OWT classification provides a practical basis for selecting regime-specific retrieval approaches in ocean color remote sensing (OCRS) (Figure A3). Incorporating OWT-dependent parameterizations may therefore reduce retrieval bias and improve estimates of carbon and sediment dynamics across optically complex river–sea systems (Hieronymi et al., 2026).

Together, the observed shifts in optical regimes (Fig. 5) and the emergence of non-linear cross-compartment bio-optical relationships (Fig. 6) demonstrate how land-sea connectivity controls both the biogeochemical and optical structure of Arctic coastal waters. With continued warming, enhanced runoff, permafrost thaw, and coastal erosion are likely to intensify sediment and OC delivery, potentially amplifying variability in optical conditions across the fluvial-marine transition zone. Integrating spatially resolved in situ observations with OWT-informed remote sensing approaches offers a pathway to capture these transitions at synoptic scales, improving the robustness of DOC, POC, and SPM retrievals in optically complex Arctic environments. These findings highlight that accurate monitoring of terrestrial matter transport on Arctic shelves requires frameworks that account for evolving optical regimes rather than relying on static regional calibrations.

5. Conclusion



Distribution and transformation of OC and suspended sediments across the Mackenzie River Delta-Beaufort Sea land-ocean interface are shaped by strong spatial transitions in hydrodynamic, biogeochemical, and optical water types. By using a compartmental framework applicable to other Arctic deltaic systems on a synthesized multi-year dataset (2009-2024), we show that DOC, POC, and SPM concentrations vary spatially and seasonally across river, delta, coastal, and marine compartments, reflecting distinct regimes of biogeochemical processing along the fluvial-marine continuum.

As water flow moves through the delta into the coastal waters and increases in salinity, DOC and POC drop and the ratio of DOC to POC increases. Across this fluvial-marine continuum, bio-optical relationships that appear linear within individual environments become non-linear when evaluated synoptically, reflecting shifts in DOM composition and particle regimes rather than measurement uncertainty. These findings indicate that remote sensing retrievals in Arctic coastal waters require calibrations spanning the full range of optical conditions. For this reason, optical water type classification provides a complement to classifying the fluvial-marine continuum, for interpreting these transitions and guiding algorithm selection in optically complex environments.

The framework applied here represents a necessary simplification of a highly heterogeneous Arctic river-sea system given still-limited in situ observations. The strong spatial variability of, especially, particulate matter further indicates that point-based sampling alone cannot fully resolve organic carbon distributions across deltaic and plume environments. Synoptic ocean-color remote sensing therefore offers a critical complementary perspective, capturing spatial gradients and evolving optical regimes that underpin cross-continuum carbon dynamics.

Appendices

585

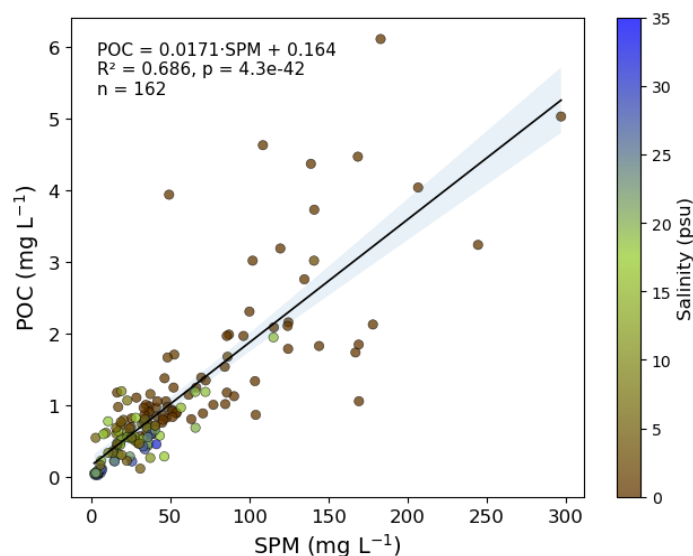




Fig. A3. In situ remote sensing reflectance (R_{rs}) observations normalized to $R_{rs}(555)$ nm from MALINA, Nunataryuk, PeCaBeau, and FLOCHAR sampling campaigns. This figure shows that the OWT classification applied in this study can
600 distinguish R_{rs} spectra very well.

Data availability

Data can be found at the links provided or by the corresponding author upon request. Nunataryuk
(<https://doi.pangaea.de/10.1594/PANGAEA.937587>); PeCaBeau (<https://doi.pangaea.de/10.1594/PANGAEA.979687>);
Mackenzie River monitoring (<https://doi.pangaea.de/10.1594/PANGAEA.988065>); and MALINA (
605 <https://doi.org/10.17882/75345>)

Author contributions

BJ, PPO, planned the campaign; AM, BJ, MH, RR performed measurements; AM, BJ, MH, RR, JL, and LB analyzed the data;
AM, BJ, PPO, RR, and MH wrote the manuscript draft; GG, JL, LB, AM, and IO reviewed and edited the manuscript.

Competing interests

610 The authors declare that they have no conflict of interest.

Disclaimer

Publications remains neutral with regard to jurisdictional claims made in the text, published maps, institutional affiliations, or
any other geographical representation in this paper. While Copernicus Publications makes every effort to include appropriate
place names, the final responsibility lies with the authors. Views expressed in the text are those of the authors and do not
615 necessarily reflect the views of the publisher.

Acknowledgements

We thank all participants of the expeditions and persons involved in the logistical support and measurements of the samples,
including Atsushi Matsuoka, Felica Gehde, Antje Eulenberg, and Maddie Santos. This project was made possible through the
620 tremendous support of the Aurora Research Institute (ARI), the hunters and trappers committees, the hamlet and town councils,
the community corporations, as well as several members of the communities of Aklavik, Inuvik and Tuktoyaktuk.



Financial support

This work was supported by the BNP Paribas Foundation Climate & Biodiversity Initiative (FLO CHAR project) and partially funded through Transnational Access of the H2020 project INTERACT (Grant Agreement No. 871120).

625 References

Arctic Great Rivers Observatory, ArcticGRO Water Quality Dataset, Absorbance Dataset, Version 20250402.

Accessed from: <https://www.arcticgreatrivers.org/data>

Circum-Arctic Map of Permafrost and Ground-Ice Conditions, Version 2 | National Snow and Ice Data Center: <https://nsidc.org/data/ggd318/versions/2>, last access: 19 February 2026.

630 Bertin, C., Carroll, D., Menemenlis, D., Dutkiewicz, S., Zhang, H., Matsuoka, A., Tank, S., Manizza, M., Miller, C. E., Babin, M., Mangin, A., and Le Fouest, V.: Biogeochemical River Runoff Drives Intense Coastal Arctic Ocean CO₂ Outgassing, *Geophys. Res. Lett.*, 50, e2022GL102377, <https://doi.org/10.1029/2022GL102377>, 2023.

635 Bertin, C., Le Fouest, V., Carroll, D., Dutkiewicz, S., Menemenlis, D., Matsuoka, A., Manizza, M., and Miller, C. E.: Terrestrial browning from Colored Dissolved Organic Matter (CDOM) changes the seasonal phenology of the coastal Arctic carbon cycle, *EGUsphere*, 1–33, <https://doi.org/10.5194/egusphere-2025-973>, 2025.

Bi, S. and Hieronymi, M.: Holistic optical water type classification for ocean, coastal, and inland waters, *Limnol. Oceanogr.*, 69, 1547–1561, <https://doi.org/10.1002/lno.12606>, 2024.

640 Biskaborn, B. K., Smith, S. L., Noetzi, J., Matthes, H., Vieira, G., Streletskiy, D. A., Schoeneich, P., Romanovsky, V. E., Lewkowitz, A. G., Abramov, A., Allard, M., Boike, J., Cable, W. L., Christiansen, H. H., Delaloye, R., Diekmann, B., Drozdov, D., Etzelmüller, B., Grosse, G., Guglielmin, M., Ingeman-Nielsen, T., Isaksen, K., Ishikawa, M., Johannsson, M., Johannsson, H., Joo, A., Kaverin, D., Kholodov, A., Konstantinov, P., Kröger, T., Lambiel, C., Lanckman, J. P., Luo, D., Malkova, G., Meiklejohn, I., Moskalenko, N., Oliva, M., Phillips, M., Ramos, M., Sannel, A. B. K., Sergeev, D., Seybold, C., Skryabin, P., Vasiliev, A., Wu, Q., Yoshikawa, K., Zheleznyak, M., and Lantuit, H.: Permafrost is warming at a global scale, *Nature Communications* 2019 10:1, 10, 264-, <https://doi.org/10.1038/s41467-018-08240-4>, 2019.

645 Burd, A. B. and Jackson, G. A.: Particle aggregation, *Ann. Rev. Mar. Sci.*, 1, 65–90, <https://doi.org/10.1146/annurev.marine.010908.163904>, 2009.

650 Chalov, S., Prokopeva, K., Magritsky, D., Grigoriev, V., Fingert, E., Habel, M., Juhls, B., Morgenstern, A., Overduin, P. P., and Kasimov, N.: Climate change impacts on streamflow, sediment load and carbon fluxes in the Lena River delta, *Ecol. Indic.*, 157, 111252, <https://doi.org/10.1016/j.ecolind.2023.111252>, 2023.

Clark, J. B., Mannino, A., Tzortziou, M., Spencer, R. G. M., and Hernes, P.: The Transformation and Export of Organic Carbon Across an Arctic River-Delta-Ocean Continuum, *J. Geophys. Res. Biogeosci.*, 127, e2022JG007139, <https://doi.org/10.1029/2022JG007139>, 2022.



- 655 Douglas, M. M., Miller, K. L., Schmeer, M. N., and Lamb, M. P.: Ablation-Limited Erosion Rates of Permafrost Riverbanks, *J. Geophys. Res. Earth Surf.*, 128, e2023JF007098, <https://doi.org/10.1029/2023JF007098>, 2023.
- Doxaran, D., Ehn, J., Bélanger, S., Matsuoka, A., Hooker, S., and Babin, M.: Optical characterisation of suspended particles in the Mackenzie River plume (Canadian Arctic Ocean) and implications for ocean colour remote sensing, *Biogeosciences*, 9, 3213–3229, <https://doi.org/10.5194/bg-9-3213-2012>, 2012.
- 660 Doxaran, D., Devred, E., and Babin, M.: A 50 % increase in the mass of terrestrial particles delivered by the Mackenzie River into the Beaufort Sea (Canadian Arctic Ocean) over the last 10 years, *Biogeosciences*, 12, 3551–3565, <https://doi.org/10.5194/bg-12-3551-2015>, 2015.
- Dupouy, C., Röttgers, R., and Doxaran, D.: Quantitative filter technique measurements of spectral light absorption by aquatic particles using a portable integrating cavity absorption meter (QFT-ICAM), *Optics Express*, Vol. 24, Issue 2, pp. A1–A20, 24, A1–A20, <https://doi.org/10.1364/oe.24.0000a1>, 2016.
- 665 Eisma, D.: Flocculation and de-flocculation of suspended matter in estuaries, *Netherlands Journal of Sea Research*, 20, 183–199, [https://doi.org/10.1016/0077-7579\(86\)90041-4](https://doi.org/10.1016/0077-7579(86)90041-4), 1986.
- Elshamy, M., Pomeroy, J. W., Pietroniro, A., Wheeler, H., Abdelhamed, M., and Davison, B.: Land surface hydrological modelling of the Mackenzie River Basin: Parametrization to simulate streamflow and permafrost dynamics, *J. Hydrol. (Amst.)*, 659, 133134, <https://doi.org/10.1016/j.jhydrol.2025.133134>, 2025.
- 670 Emmerton, C. A., Lesack, L. F. W., and Vincent, W. F.: Mackenzie River nutrient delivery to the Arctic Ocean and effects of the Mackenzie Delta during open water conditions, *Global Biogeochem. Cycles*, 22, <https://doi.org/10.1029/2006GB002856>, 2008.
- Grunert, B. K., Tzortziou, M., Neale, P., Menendez, A., and Hernes, P.: DOM degradation by light and microbes along the Yukon River-coastal ocean continuum, *Scientific Reports* 2021 11:1, 11, 10236-, <https://doi.org/10.1038/s41598-021-89327-9>, 2021.
- 675 Hernes, P. J. and Benner, R.: Photochemical and microbial degradation of dissolved lignin phenols: Implications for the fate of terrigenous dissolved organic matter in marine environments, *J. Geophys. Res. Oceans*, 108, <https://doi.org/10.1029/2002jc001421>, 2003.
- Hieronymi, M., Behr, D., Bi, S., and Röttgers, R.: Optical complexity of North Sea, Baltic Sea, and adjacent coastal and inland waters derived from Sentinel-3 OLCI satellite data, *Earth Syst. Sci. Data*, 18, 1307–1329, <https://doi.org/10.5194/essd-18-1307-2026>, 2026.
- 680 Holmes, R. M., McClelland, J. W., Peterson, B. J., Tank, S. E., Bulygina, E., Eglinton, T. I., Gordeev, V. V., Gurtovaya, T. Y., Raymond, P. A., Repeta, D. J., Staples, R., Striegl, R. G., Zhulidov, A. V., Zimov, S. A., Holmes, R. M., Bulygina, E., McClelland, J. W., Peterson, B. J., Tank, S. E., Gordeev, V. V., Shirshov, P. P., Gurtovaya, T. Y., Zhulidov, A. V.,
- 685 Raymond, P. A., Repeta, D. J., Staples, R., Striegl, R. G., and Zimov, S. A.: Seasonal and Annual Fluxes of Nutrients and Organic Matter from Large Rivers to the Arctic Ocean and Surrounding Seas, *Estuaries and Coasts* 2011 35:2, 35, 369–382, <https://doi.org/10.1007/s12237-011-9386-6>, 2011.



- 690 Irrgang, A. M., Bendixen, M., Farquharson, L. M., Baranskaya, A. V., Erikson, L. H., Gibbs, A. E., Ogorodov, S. A.,
Overduin, P. P., Lantuit, H., Grigoriev, M. N., and Jones, B. M.: Drivers, dynamics and impacts of changing Arctic
coasts, *Nature Reviews Earth & Environment* 2022 3:1, 3, 39–54, <https://doi.org/10.1038/s43017-021-00232-1>, 2022.
- Juhls, B., Paul Overduin, P., Hölemann, J., Hieronymi, M., Matsuoka, A., Heim, B., and Fischer, J.: Dissolved organic
matter at the fluvial-marine transition in the Laptev Sea using in situ data and ocean colour remote sensing,
Biogeosciences, 16, 2693–2713, <https://doi.org/10.5194/bg-16-2693-2019>, 2019.
- 695 Juhls, B., Matsuoka, A., Lizotte, M., Bécu, G., Overduin, P. P., El Kassar, J., Devred, E., Doxaran, D., Ferland, J., Forget,
M. H., Hilborn, A., Hieronymi, M., Leymarie, E., Maury, J., Oziel, L., Tisserand, L., Anikina, D. O. J., Dillon, M., and
Babin, M.: Seasonal dynamics of dissolved organic matter in the Mackenzie Delta, Canadian Arctic waters: Implications
for ocean colour remote sensing, *Remote Sens. Environ.*, 283, 113327, <https://doi.org/10.1016/j.rse.2022.113327>, 2022.
- Keil, R. G., Mayer, L. M., Quay, P. D., Richey, J. E., and Hedges, J. I.: Loss of organic matter from riverine particles in
deltas, *Geochim. Cosmochim. Acta*, 61, 1507–1511, [https://doi.org/10.1016/S0016-7037\(97\)00044-6](https://doi.org/10.1016/S0016-7037(97)00044-6), 1997.
- 700 Lattaud, J., Aichner, B., Gierga, M., Stolz, A., Meętrak, M., Wilk, M., Suska-Malawska, M., Mischke, S., Sachse, Di.,
Rajabov, I., Rajabov, N., and Rethemeyer, J.: Biomarker ¹⁴C evidence for sources and recycling of pre-aged organic
carbon in Arctic permafrost regions, *Geochim. Cosmochim. Acta*, 393, 75–85, <https://doi.org/10.1017/RDC.2021.78>,
2025.
- Lizotte, M., Juhls, B., Matsuoka, A., Massicotte, P., Mével, G., Anikina, D. O. J., Antonova, S., Bécu, G., Béguin, M.,
705 Bélanger, S., Bossé-Demers, T., Bröder, L., Bruyant, F., Chaillou, G., Comte, J., Couture, R. M., Devred, E.,
Deslongchamps, G., Dezutter, T., Dillon, M., Doxaran, D., Flamand, A., Fell, F., Ferland, J., Forget, M. H., Fritz, M.,
Gordon, T. J., Guilmette, C., Hilborn, A., Husserr, R., Irish, C., Joux, F., Kipp, L., Laberge-Carignan, A., Lantuit, H.,
Leymarie, E., Mannino, A., Maury, J., Overduin, P., Oziel, L., Stedmon, C., Thomas, C., Tisserand, L., Tremblay, J. É.,
Vonk, J., Whalen, D., and Babin, M.: Nunataryuk field campaigns: understanding the origin and fate of terrestrial organic
710 matter in the coastal waters of the Mackenzie Delta region, *Earth Syst. Sci. Data*, 15, <https://doi.org/10.5194/essd-15-1617-2023>, 2023.
- Lynch, L. M., Machmuller, M. B., Boot, C. M., Covino, T. P., Rithner, C. D., Cotrufo, M. F., Hoyt, D. W., and
Wallenstein, M. D.: Dissolved Organic Matter Chemistry and Transport Along an Arctic Tundra Hillslope, *Global
Biogeochem. Cycles*, 33, 47–62, <https://doi.org/10.1029/2018GB006030>, 2019.
- 715 Mann, P. J., Davydova, A., Zimov, N., Spencer, R. G. M., Davydov, S., Bulygina, E., Zimov, S., and Holmes, R. M.:
Controls on the composition and lability of dissolved organic matter in Siberia’s Kolyma River basin, *J. Geophys. Res.
Biogeosci.*, 117, <https://doi.org/10.1029/2011JG001798>, 2012.
- Mann, P. J., Spencer, R. G. M., Hernes, P. J., Six, J., Aiken, G. R., Tank, S. E., McClelland, J. W., Butler, K. D., Dyda,
R. Y., and Holmes, R. M.: Pan-arctic trends in terrestrial dissolved organic matter from optical measurements, *Front.
720 Earth Sci. (Lausanne)*, 4, 171139, <https://doi.org/10.3389/feart.2016.00025>, 2016.



- 725 Massicotte, P., Amon, R. M. W., Antoine, D., Archambault, P., Balzano, S., Bélanger, S., Benner, R., Boeuf, D., Bricaud, A., Bruyant, F., Chaillou, G., Chami, M., Charrière, B., Chen, J., Claustre, H., Coupel, P., Delsaut, N., Doxaran, D., Ehn, J., Fichot, C., Forget, M. H., Fu, P., Gagnon, J., Garcia, N., Gasser, B., Ghiglione, J. F., Gorsky, G., Gosselin, M., Gourvil, P., Gratton, Y., Guillot, P., Heipieper, H. J., Heussner, S., Hooker, S. B., Huot, Y., Jeanthon, C., Jeffrey, W., Joux, F., Kawamura, K., Lansard, B., Leymarie, E., Link, H., Lovejoy, C., Marec, C., Marie, D., Martin, J., Martín, J., Massé, G., Matsuoka, A., McKague, V., Mignot, A., Miller, W. L., Miquel, J. C., Mucci, A., Ono, K., Ortega-Retuerta, E., Panagiotopoulos, C., Papakyriakou, T., Picheral, M., Prieur, L., Raimbault, P., Ras, J., Reynolds, R. A., Rochon, A., Rontani, J. F., Schmechtig, C., Schmidt, S., Sempéré, R., Shen, Y., Song, G., Stramski, D., Tachibana, E., Thirouard, A., Tolosa, I., Tremblay, J. E., Vaïtilingom, M., Vaultot, D., Vaultier, F., Volkman, J. K., Xie, H., Zheng, G., and Babin, M.: The MALINA oceanographic expedition: How do changes in ice cover, permafrost and UV radiation impact biodiversity and biogeochemical fluxes in the Arctic Ocean?, *Earth Syst. Sci. Data*, 13, 1561–1592, <https://doi.org/10.5194/essd-13-1561-2021>, 2021.
- 730 Matsuoka, A., Bricaud, A., Benner, R., Para, J., Sempéré, R., Prieur, L., Bélanger, S., and Babin, M.: Tracing the transport of colored dissolved organic matter in water masses of the Southern Beaufort Sea: relationship with hydrographic characteristics, *Biogeosciences*, 9, 925–940, <https://doi.org/10.5194/bg-9-925-2012>, 2012.
- 735 Matsuoka, A., Hooker, S. B., Bricaud, A., Gentili, B., and Babin, M.: Estimating absorption coefficients of colored dissolved organic matter (CDOM) using a semi-analytical algorithm for southern Beaufort Sea waters: Application to deriving concentrations of dissolved organic carbon from space, *Biogeosciences*, 10, 917–927, <https://doi.org/10.5194/bg-10-917-2013>, 2013.
- 740 Matsuoka, A., Boss, E., Babin, M., Karp-Boss, L., Hafez, M., Chekalyuk, A., Proctor, C. W., Werdell, P. J., and Bricaud, A.: Pan-Arctic optical characteristics of colored dissolved organic matter: Tracing dissolved organic carbon in changing Arctic waters using satellite ocean color data, *Remote Sens. Environ.*, 200, 89–101, <https://doi.org/10.1016/j.rse.2017.08.009>, 2017.
- 745 Matsuoka, A., Babin, M., and Vonk, J. E.: Decadal trends in the release of terrigenous organic carbon to the Mackenzie Delta (Canadian Arctic) using satellite ocean color data (1998–2019), *Remote Sens. Environ.*, 283, 113322, <https://doi.org/10.1016/j.rse.2022.113322>, 2022.
- 750 McClelland, J. W., Holmes, R. M., Peterson, B. J., Raymond, P. A., Striegl, R. G., Zhulidov, A. V., Zimov, S. A., Zimov, N., Tank, S. E., Spencer, R. G. M., Staples, R., Gurtovaya, T. Y., and Griffin, C. G.: Particulate organic carbon and nitrogen export from major Arctic rivers, *Global Biogeochem. Cycles*, 30, 629–643, <https://doi.org/10.1002/2015GB005351>, 2016.
- Moran, M. A., Ferrer-González, F. X., Fu, H., Nowinski, B., Olofsson, M., Powers, M. A., Schreier, J. E., Schroer, W. F., Smith, C. B., and Uchimiya, M.: The Ocean’s labile DOC supply chain, *Limnol. Oceanogr.*, 67, 1007–1021, <https://doi.org/10.1002/lno.12053>, 2022.



- Morgenstern, A. and Gottschalk, M.: Berichte zur Polar- und Meeresforschung, Bericht Nr. 797/2025, 2023, https://doi.org/10.57738/BzPM_0797_2025, 2023.
- Nielsen, D. M., Pieper, P., Barkhordarian, A., Overduin, P., Ilyina, T., Brovkin, V., Baehr, J., and Dobrynin, M.: Increase in Arctic coastal erosion and its sensitivity to warming in the twenty-first century, *Nature Climate Change* 2022 12:3, 12, 263–270, <https://doi.org/10.1038/s41558-022-01281-0>, 2022.
- Novak, M. G., Mannino, A., Clark, J. B., Hernes, P., Tzortziou, M., Spencer, R. G. M., Kellerman, A. M., and Grunert, B.: Arctic biogeochemical and optical properties of dissolved organic matter across river to sea gradients, *Front. Mar. Sci.*, 9, 949034, <https://doi.org/10.3389/fmars.2022.949034>, 2022.
- Ogneva, O., Mollenhauer, G., Juhls, B., Sanders, T., Palmtag, J., Fuchs, M., Grotheer, H., Mann, P. J., and Strauss, J.: Particulate organic matter in the Lena River and its delta: from the permafrost catchment to the Arctic Ocean, *Biogeosciences*, 20, 1423–1441, <https://doi.org/10.5194/bg-20-1423-2023>, 2023.
- van Oostende, M., Hieronymi, M., Krasemann, H., and Baschek, B.: Global ocean colour trends in biogeochemical provinces, *Front. Mar. Sci.*, 10, 1052166, <https://doi.org/10.3389/fmars.2023.1052166>, 2023.
- Oziel, L., Gürses, Ö., Torres-Valdés, S., Hoppe, C. J. M., Rost, B., Karakuş, O., Danek, C., Koch, B. P., Nissen, C., Koldunov, N., Wang, Q., Völker, C., Iversen, M., Juhls, B., and Hauck, J.: Climate change and terrigenous inputs decrease the efficiency of the future Arctic Ocean’s biological carbon pump, *Nature Climate Change* 2025 15:2, 15, 171–179, <https://doi.org/10.1038/s41558-024-02233-6>, 2025.
- Pegau, W. S., Gray, D., and Zaneveld, J. R. V.: Absorption and attenuation of visible and near-infrared light in water: dependence on temperature and salinity, *Appl. Opt.*, 36, 6035, <https://doi.org/10.1364/ao.36.006035>, 1997.
- Peterson, B. J., Holmes, R. M., McClelland, J. W., Vörösmarty, C. J., Lammers, R. B., Shiklomanov, A. I., Shiklomanov, I. A., and Rahmstorf, S.: Increasing river discharge to the Arctic Ocean, *Science*, 298, 2171–2173, <https://doi.org/10.1126/science.1077445>, 2002.
- Pugach, S. P., Pipko, I. I., Shakhova, N. E., Shirshin, E. A., Perminova, I. V., Gustafsson, Ö., Bondur, V. G., Ruban, A. S., and Semiletov, I. P.: Dissolved organic matter and its optical characteristics in the Laptev and East Siberian seas: Spatial distribution and interannual variability (2003–2011), *Ocean Science*, 14, 87–103, <https://doi.org/10.5194/os-14-87-2018>, 2018.
- Rantanen, M., Karpechko, A. Y., Lipponen, A., Nordling, K., Hyvärinen, O., Ruosteenoja, K., Vihma, T., and Laaksonen, A.: The Arctic has warmed nearly four times faster than the globe since 1979, *Communications Earth & Environment* 2022 3:1, 3, 168-, <https://doi.org/10.1038/s43247-022-00498-3>, 2022.
- Rapaić, M., Brown, R., Markovic, M., Chaumont, D., and Rapaić, M. R.: An Evaluation of Temperature and Precipitation Surface-Based and Reanalysis Datasets for the Canadian Arctic, *Atmosphere-Ocean*, 53, 283–303, <https://doi.org/10.1080/07055900.2015.1045825>, 2015.



Röttgers, R. and Doerffer, R.: Measurements of optical absorption by chromophoric dissolved organic matter using a point-source integrating-cavity absorption meter, *Limnol. Oceanogr. Methods*, 5, 126–135, <https://doi.org/10.4319/lom.2007.5.126>, 2007.

790 Röttgers, R., McKee, D., and Utschig, C.: Temperature and salinity correction coefficients for light absorption by water in the visible to infrared spectral region, *Opt. Express*, 22, 25093–25108, <https://doi.org/10.1364/oe.22.025093>, 2014.

Röttgers, R., Doxaran, D., and Dupouy, C.: Quantitative filter technique measurements of spectral light absorption by aquatic particles using a portable integrating cavity absorption meter (QFT-ICAM), *Opt. Express*, 24, A1, <https://doi.org/10.1364/oe.24.0000a1>, 2015.

795 Schuur, E. A. G., McGuire, A. D., Schädel, C., Grosse, G., Harden, J. W., Hayes, D. J., Hugelius, G., Koven, C. D., Kuhry, P., Lawrence, D. M., Natali, S. M., Olefeldt, D., Romanovsky, V. E., Schaefer, K., Turetsky, M. R., Treat, C. C., and Vonk, J. E.: Climate change and the permafrost carbon feedback, *Nature* 2015 520:7546, 520, 171–179, <https://doi.org/10.1038/nature14338>, 2015.

Sholkovitz, E. R.: Flocculation of dissolved organic and inorganic matter during the mixing of river water and seawater, *Geochim. Cosmochim. Acta*, 40, 831–845, [https://doi.org/10.1016/0016-7037\(76\)90035-1](https://doi.org/10.1016/0016-7037(76)90035-1), 1976.

800 Sullivan, J. M., Twardowski, M. S., Zaneveld, J. R. V., Moore, C. M., Barnard, A. H., Donaghay, P. L., and Rhoades, B.: Hyperspectral temperature and salt dependencies of absorption by water and heavy water in the 400–750 nm spectral range, *Applied Optics*, Vol. 45, Issue 21, pp. 5294–5309, 45, 5294–5309, <https://doi.org/10.1364/AO.45.005294>, 2006.

805 Tank, S. E., Striegl, R. G., McClelland, J. W., and Kokelj, S. V.: Multi-decadal increases in dissolved organic carbon and alkalinity flux from the Mackenzie drainage basin to the Arctic Ocean, *Environmental Research Letters*, 11, 054015, <https://doi.org/10.1088/1748-9326/11/5/054015>, 2016.

Tarasenko, A., Doxaran, D., and Gentili, B.: Variations of suspended particulate matter concentrations of the Mackenzie River plume (Beaufort Sea, Arctic Ocean) over the last two decades, *Mar. Pollut. Bull.*, 196, 115619, <https://doi.org/10.1016/j.marpolbul.2023.115619>, 2023.

810 Tassan, S. and Ferrari, G. M.: Proposal for the measurement of backward and total scattering by mineral particles suspended in water, *Appl. Opt.*, 34, 8345, <https://doi.org/10.1364/ao.34.008345>, 1995.

Tassan, S. and Ferrari, G. M.: A sensitivity analysis of the “Transmittance - Reflectance” method for measuring light absorption by aquatic particles, *J. Plankton Res.*, 24, 757–774, <https://doi.org/10.1093/plankt/24.8.757>, 2002.

815 Vonk, J. E., Tank, S. E., Bowden, W. B., Laurion, I., Vincent, W. F., Alekseychik, P., Amyot, M., Billet, M. F., Canário, J., Cory, R. M., Deshpande, B. N., Helbig, M., Jammet, M., Karlsson, J., Larouche, J., Macmillan, G., Rautio, M., Walter Anthony, K. M., and Wickland, K. P.: Reviews and syntheses: Effects of permafrost thaw on Arctic aquatic ecosystems, *Biogeosciences*, 12, 7129–7167, <https://doi.org/10.5194/bg-12-7129-2015>, 2015.

Walker, S. A., Amon, R. M. W., and Stedmon, C. A.: Variations in high-latitude riverine fluorescent dissolved organic matter: A comparison of large Arctic rivers, *J. Geophys. Res. Biogeosci.*, 118, 1689–1702, <https://doi.org/10.1002/2013JG002320>, 2013.



- 820 Ward, C. P., Nalven, S. G., Crump, B. C., Kling, G. W., and Cory, R. M.: Photochemical alteration of organic carbon draining permafrost soils shifts microbial metabolic pathways and stimulates respiration, *Nature Communications* 2017 8:1, 8, 772-, <https://doi.org/10.1038/s41467-017-00759-2>, 2017.
- Xi, H., Larouche, P., Tang, S., and Michel, C.: Seasonal variability of light absorption properties and water optical constituents in Hudson Bay, Canada, *J. Geophys. Res. Oceans*, 118, 3087–3102, <https://doi.org/10.1002/jgrc.20237>,
825 2013.
- Zhang, R., Wang, H., Fu, Q., Rasch, P. J., Wu, M., and Maslowski, W.: Understanding the Cold Season Arctic Surface Warming Trend in Recent Decades, *Geophys. Res. Lett.*, 48, e2021GL094878, <https://doi.org/10.1029/2021GL094878>, 2021.